UNIVERSIDAD NACIONAL AUTONOMA DE MEXICO
MAESTRÍA EN CIENCIAS (FÍSICA)
INSTITUTO DE FÍSICA
FÍSICA DE ALTAS ENERGÍAS

EFFECTS OF FINITE WIDTH ON ANOMALOUS CHIRAL PROCESSES

TESIS
QUE PARA OPTAR POR EL GRADO DE:
MAESTRO EN CIENCIAS (FÍSICA)

PRESENTA:
ESPARZA ARELLANO LEONARDO

TUTOR PRINCIPAL:
DR. GENARO TOLEDO SÁNCHEZ
INSTITUTO DE FÍSICA

MIEMBROS DEL COMITÉ TUTOR:
DR. ROELOF BIJKER BIJKER
INSTITUTO DE CIENCIAS NUCLEARES
DR. LUIS ARMANDO ACOSTA SÁNCHEZ
INSTITUTO DE FÍSICA

CD. MX. JUNIO 2023

Agradecimientos

A mis amigos, especialmente a mi amigo Damián, quienes me motivaron a alcanzar mi sueño de convertirme en físico, sin importar todas las cosas a las que tuve que renunciar para lograrlo.

A mi mamá y toda mi familia, quienes nunca han dejado de creer en mí y me apoyan con su afecto y compañía.

A mi tutor el Dr. Genaro Toledo Sánchez, quien fue un gran mentor durante mi trayectoria como estudiante de maestría, así como en la realización de este trabajo.

A todos mis seres queridos que perdí durante esta pandemia, incluyendo a mis tíos Damián y Jorge y a mi primo Adrián.

Al Instituto de Física de la UNAM y sus académicos por brindarme la oportunidad de cursar este posgrado.

Summary

Hadronic states are the relevant degrees of freedom from the strong interaction at low energies. In this regime, it is possible to make an accurate description of hadronic processes using effective theories, which involve effective coupling constants between hadrons. Such couplings summarize internal processes, which include the kinematical conditions at which hadrons are tied up. One of such conditions is the so-called "mass shell" condition, in which a state can be on-shell or off-shell. The deviation of states with respect to their mass shell is parameterized by its finite decay width.

Some of the question that arises from this formalism are: What is the effect of the finite decay width of intermediate states in an experimental observation? Are the coupling constants sensible to those effects?

In this work, these questions are addressed considering the particular anomalous process $\pi^0 \to \gamma\gamma$ which, from an effective theory point of view, can be seen as mediated by the interaction between mesons π^0, ρ^0, ω^0 in a vectorial dominance approximation. This is parameterized by the effective coupling constant $g_{\rho\omega\pi}$.

In order to explore the effects of finite width of ρ and ω states, the scattering process $e^+e^- \to \pi^0\pi^0\gamma$ is considered, which in its intermediate states includes two of the anomalous vertices described above.

Considering the angular distribution of one of the pions final state as an observable, then the effects of the finite width can be explored on different kinematical conditions, as well as the contributions coming from re-scattering processes in the couplings. These re-scattering effects on the $g_{\rho\omega\pi}$ coupling constant are calculated for the general case where both photons final state are off-shell, and for the case where only one of them is off-shell and the other one is on-shell.

Just as comparative examples, the Higgs decay processes $H \to \gamma\gamma$ and $H \to l\bar{l}l\bar{l}$ are presented. Even though Higgs decay and pion decay processes are

different and have nothing to do with one another, their intermediate states are relevant in both scenarios.

Results demonstrate re-scattering correction is significant when both final particles are on-shell, and not relevant in the mixed scenario on-shell off-shell. Both ρ and ω states are observed, and it is clear how sensible the observables are to their finite decay widths, which are energy dependent. Also, the angular distribution shows a direct dependence on coupling constant and finite decay widths.

Contents

6

Chapter 1

Motivation and Specific objectives

1.1 Motivation

Higgs discovery was lead by a series of experiments [1] which were not intended to look for the Higgs directly, but for processes where the Higgs could manifest itself as a resonance, like Higgs decaying into two photons $H \rightarrow \gamma\gamma$ and Higgs decaying into four leptons $H \rightarrow ZZ^* \rightarrow l\bar{l}l\bar{l}$.

Unlike the Higgs boson being a scalar particle, pions are pseudoscalar particles with well-studied properties (mass, decay width, decay modes, lifetime). Both particles share similar decay modes $H \rightarrow \gamma\gamma$ and $\pi^0 \rightarrow \gamma\gamma$ in the sense that both decay into two photons via loop mechanism. However, the Higgs decay is just as comparative model used in this work, they are not the same decays.

Pion decay into two photons $\pi^0 \rightarrow \gamma\gamma$ is only possible thanks to an anomalous term, often referred to as an *anomaly*, which implies the violation of Ward Identities (Anomalous Ward Identities), otherwise, this process would be highly suppressed.

Even though pion decay into two photons $\pi^0 \rightarrow \gamma\gamma$ is a well-studied process, applying a similar analysis employed on $H \rightarrow \gamma\gamma$, plus some hadronic physics and effective models, this work aims to explore the appearance of hadronic resonances inside the corrective loop at low energies, which implies studying effective couplings such as $g_{\rho\omega\pi}, g_{V\pi\gamma}, g_{V\gamma}$ and analyze the effect of their finite width in the cross section.

Among the literature one can find works with different formalism (like the Schwinger-Dyson equations) describing the pion form factor [2, 3, 4], nonetheless, they cover a much wider range of energies, which have diverse applications.

1.2   Specific objectives

- Obtain an energy-dependent expression of the coupling constant $g_{\rho\omega\pi}$ from the pion decay $\pi^0 \rightarrow \gamma\gamma$, with intermediate meson states ρ, ω and argue when re-scattered correction acquires relevance.

- Apply this last expression to scattering process $e^+e^- \rightarrow \pi^0\pi^0\gamma$, where two vertices involving the $g_{\rho\omega\pi}$ coupling constant take place. Analyze its differential cross section and give a proper interpretation of its dependence on parameters like decay widths $\Gamma_\rho, \Gamma_\omega$ (which are energy-dependent as well) and scattered angle θ of final particles (angle of one of the final state pions measured from the e^+e^- center of mass frame).

- Discuss how the likeness of ρ and ω masses gives rise to a mixed resonant state of both vectorial propagators D_ρ, D_ω (modulated by decay widths $\Gamma_\rho, \Gamma_\omega$), giving as a result an amplified cross section.

Using Vector Meson Dominance model, the main purpose of this work is to propose an additional term to the amplitude of the pion decay $\pi \rightarrow \gamma\gamma$, generalize its initial conditions in order to apply it to the particular scattering channel $e^+e^- \rightarrow \pi^0\pi^0\gamma$, test whether or not this correction makes a significant contribution and analyze how the manipulation of the different properties of ρ, ω resonances influence the angular distribution.
With these objectives in mind, the present work is divided as follows:
In Chapter 2, a brief summary of particle physics is introduced, which includes standard model phenomenology, hadronic physics, the eightfold way, Feynman rules for *Quantum Electrodynamics* (QED) and *Vector Meson Dominance* (VMD) effective model.
Chapter 3 introduces some symmetry concepts such as Noether's theorem, spontaneous symmetry breaking and some particular examples of interest for this thesis, among which are the Goldstone theorem, sigma model, PCAC. The chapter ends with the introduction of anomalous Ward Identities and

how they give rise to the pion decay $\pi^0 \to \gamma\gamma$, and the *Wess-Zumino-Witten* (WZW) anomalous action.

Chapter 4 presents the definition of resonant particles, deduces what is known as the complex mass scheme to the propagator of unstable particles and exposes the Higgs boson decay via W and Z loop channels.

In Chapter 5 the theoretical calculations of this thesis are given, beginning with the pion decay $\pi^0 \to \gamma\gamma$ with intermediate resonant states ρ^0, ω^0 and its re-scattered process with intermediate one-loop $\rho\omega\pi$. A discussion of how the imaginary terms of the unstable particle propagators is included is also found. Finally, the corrected expression of $g_{\rho\omega\pi}(q^2)$ is given for off-shell and on-shell conditions.

In Chapter 6 the previous calculations from Chapter 5 are applied to the particular process $e^+e^- \to \pi^0\pi^0\gamma$. The differential cross section with respect to the scattered angle described above is calculated and its dependence with the different conditions stated in the specific objectives is analyzed, as well as the favored scattered angles are illustrated with plots in the results section. This thesis ends with Chapter 7, presenting the final conclusions.

Chapter 2

Basis of particle physics

This chapter gives an elementary summary of the standard model of particle physics from a phenomenological point of view; the three fundamental interactions, leptons, quarks, gauge bosons and how the eightfold way [5] explains the way quarks combine into bound states to create hadrons on SU(3) symmetry group. It also summarizes the Feynman rules of Quantum Electrodynamics (QED), as well as the Vector Meson Dominance (VMD) effective model.

2.1   Standard model phenomenology

"Phenomenology" is the part of theoretical physics that deals with the interpretation and understanding of experiments involving elementary particles. Within the Standard Model of Particle Physics, it plays an important role in on-going experiments taking place at laboratories from all around the world, such as CERN, SLAC, Fermilab, BELLE II, just to mention a few. Quantum Field Theory (QFT) is the main mathematical machinery physicist use to describe elementary particles. Built on the QFT formalism, the standard model describes the 3 fundamental interactions of nature (excluding gravity [6]):

- Electromagnetic interaction

- Weak interaction

- Strong interaction

Each interaction is mediated by force-carrying particles called *Gauge Bosons*, which have spin 1.

Interaction between particles exists in a particular field; the particles found in nature are *excitations* of every field and the gauge bosons are the force-carrying particles.

For the 3 fundamental interactions, the associated gauge bosons are the *photon* γ for the electromagnetic interaction, $W^{\pm}$ and Z^0 for the weak interaction and the *gluons* for the strong interaction.

Within QFT, the fundamental theories used to describe particle interactions are the electromagnetic, strong and weak interactions: *Quantum Electrodynamics* (QED), *Quantum Chromodynamics* (QCD) and the Electroweak Theory (also known as *Glashow-Weinberg-Salam Model*) respectively.

The particles that make up matter have spin 1/2 and are divided into two main categories: *leptons* and *quarks*.

2.1.1   Leptons and quarks

Leptons consist of six members: *electron* (e^-), *muon* (μ^-), *tau* (τ^-) and their corresponding *neutrinos*: ν_e, ν_μ, ν_τ. The first three of them carry electric charge -1 (in units of e). They interact via electromagnetic and weak forces. Neutrinos are electrically neutral, so the only way they interact is via the weak force. None of the six leptons interact via the strong force.

Quarks also consist of six members, and they come in six *flavors*: *up* (u), *down* (d), *charm* (c), *strange* (s), *top* (t), *bottom* (b). They carry electric charge $+\frac{2}{3}$ or $-\frac{1}{3}$ (in units of electric charge e) and all of them interact via the strong, weak and electromagnetic forces.

Just as electric charge is a property of the electromagnetic interaction, there is another charge associated with the strong interaction called *"color"*. There are three different color charges: *green, blue, red*. Quarks can only be arranged in such a way that the combination of colors (total color charge) is white, *i.e.* no individual quarks can exist according to QCD.

In particle physics, a particle p has it's own *antiparticle*, which is denoted with an upper bar $\bar{p}$. Antiparticles have the opposite charge of the original particle and the exact same mass.

Tables 2.1 and 2.2 list all leptons and quarks of the standard model with their corresponding electric charges and masses.

Flavor	Mass (GeV/c^2)	Charge
e^-	$5.10998928(11) \times 10^{-4}$	-1
ν_e	$< 0.2 \times 10^{-8}$	0
μ	$0.1056583715(35)$	-1
ν_μ	$< 1.9 \times 10^{-4}$	0
τ	$1.77682(16)$	-1
ν_τ	< 0.0182	0

Table 2.1: Lepton masses and their corresponding charges (in units of e).

Flavor	Mass (GeV/c^2)	Charge
u	2.55×10^{-3}	2/3
d	5.04×10^{-3}	-1/3
c	1.27	2/3
s	0.105	-1/3
t	173.4	2/3
b	4.2	-1/3

Table 2.2: Bare quark masses and their corresponding electric charges (in units of e).

2.2 Hadronic physics

2.2.1 Symmetries and groups

Group Theory is the branch of mathematics that studies algebraic structures known as *groups*. It underlies the treatment of *symmetry*, a concept that lies deep into the heart of particle physics, as will be illustrated in subsequent chapters.

In the mid-20th century, physicist began to discover many new hadrons, which led Gell-Mann and, independently, Nishijima to propose a new "periodic table" where all hadrons would be composed of the three lightest quarks *u, d, s*. This new periodic table is the $SU(3)$ multiplet of *isospin* I_3 and *hypercharge Y*, illustrated in Figure 2.1, where hypercharge is defined as the sum of the Baryon Number ($B = 1/3$ for all quarks) and Strangeness S:

$$Y = B + S. \tag{2.1}$$

The total charge Q can be obtained from the relation

$$Q = I_3 + \frac{Y}{2} \tag{2.2}$$
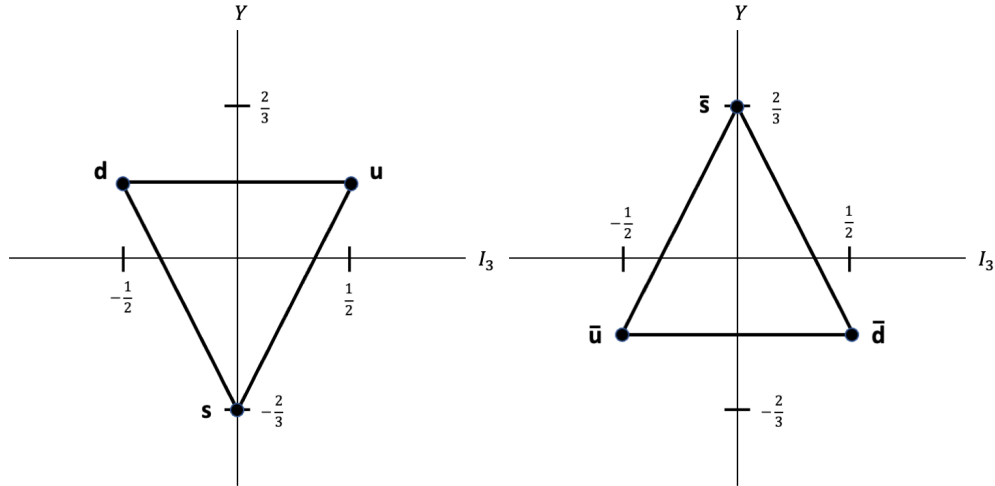
Figure 2.1: SU(3) multiplet of isospin I_3 and hypercharge Y for quarks (left) and antiquarks (right).

A summary of quark's quantum numbers can be found in Table 2.3

Quark	Spin	B	Q	I_3	S	Y
u	$\frac{1}{2}$	$\frac{1}{3}$	$\frac{2}{3}$	$\frac{1}{2}$	0	$\frac{1}{3}$
d	$\frac{1}{2}$	$\frac{1}{3}$	$-\frac{1}{3}$	$-\frac{1}{2}$	0	$\frac{1}{3}$
s	$\frac{1}{2}$	$\frac{1}{3}$	$-\frac{1}{3}$	0	-1	$-\frac{1}{3}$

Table 2.3: Quark's quantum numbers.

2.2.2 Bound states of quarks: mesons and baryons

When two or three quarks interact and form a *bound state*, they create a *hadron*. Hadrons are divided into *mesons* (a pair of quark and anti-quark denoted by $q\bar{q}$) and *baryons* (a triplet of three quarks or three anti-quarks,

13

denoted by qqq or $\bar{q}\bar{q}\bar{q}$). They can also be arranged in groups of four quarks (tetraquark) and five quarks (pentaquarks), but their properties are outside the scope of this work.

As mentioned in Section 2.1, according to QCD, hadrons will be colorless, this means mesons will consist of a pair of a quark q with a color charge (red, blue, green) and an antiquark $\bar{q}$ with his corresponding anti color charge (anti-red, anti-blue, anti-green), while baryons will consist of any qqq or $\bar{q}\bar{q}\bar{q}$ with their corresponding color charges.

By limiting this section to the light regime of QCD (that is, excluding the charm c, top t and bottom b heavy quarks) q could be an up, down or strange quark ($q = u, d, s$), this gives 9 different possibilities for mesons (where obviously $q\bar{q} = \bar{q}q$). After normalization and orthogonality, the nine states divide into a $SU(3)$ octet and a $SU(3)$ singlet. These nine states are arranged in Figure 2.2. Left diagram corresponds to *pseudoscalar mesons* with $J^{PC} = 0^{-+}$, while the one on the right corresponds to *vectorial mesons* with $J^{PC} = 1^{--}$ (where $P = -(-1)^L$ is the parity of the meson, $C = (-1)^{L+S}$ is the charge operator, $J = L + S$ is the spin of the composite meson, and L, S are the relative angular momentum and spín of q or $\bar{q}$, respectively). This arrangement and the one for baryons is known as *"The Eightfold Way"*, proposed by Gell-Mann [5] and Ne'eman [7] in 1961.
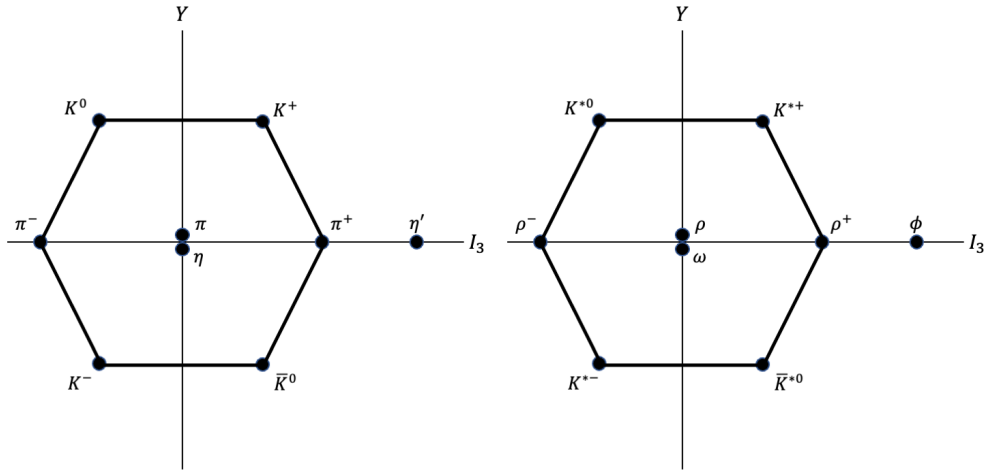

Figure 2.2: SU(3) octet and singlet of pseudoscalar mesons (left) and vectorial mesons (right).

A summary of the neutral ρ, ω and π (omitting the neutral exponent for the

sake of notation) particle properties can be found in Table 2.4

Particle	Consist of quarks	Mass (MeV)	Decay Width (MeV)
π	$\frac{u\bar{u}-d\bar{d}}{\sqrt{2}}$	134.9768	~ 0
ρ	$u\bar{u}, d\bar{d}$	775.26	149.1
ω	$u\bar{u}, d\bar{d}$	782.66	8.68

Table 2.4: Properties of neutral mesons π, ρ, ω [8].

A few comments on Table 2.4; pion decay width value is shown as zero. This is due to the fact that pion lifetime distribution is so narrowed in such a way it can be considered null in a first approach, however, its value and description will be part of this work. Also, even though ρ and ω particles have exactly the same composition of quarks ($u\bar{u}$ or $d\bar{d}$) but in different combinations and very similar masses (both particles being vectorial mesons with $Y = 0$ and $I_3 = 0$), there is a subtle difference as they have different isospin values, being $I = 1$ for the former and $I = 0$ for the latter, respectively.

Finally, comparing the values of the masses from Table 2.4 and Table 2.2, it is evident that mesons masses are larger than their constituent quarks masses. The reason of this, besides QCD interactions, has to do with the fact that light quarks (u, d, s) do not form a perfect $SU(3)$ symmetry, *i.e.* m_d is slightly larger than m_u, and m_s is significantly larger than both u and d quarks ($m_u < m_d << m_s$), this is known as *breaking of flavor symmetry* [9, 10], this explains why particles like K (containing s quark) are heavier than π.

However, particles like ρ and π with the same quark content should have the same mass, but as can be seen from Table 2.4, their masses are not exactly the same. This is explained with the fact that pseudoscalar and vectorial mesons differ only in the relative orientation of their quark spins, which creates a spin-spin interaction similar to the hyperfine splitting of the hydrogen atom and causes the difference in the mass of the mesons.

2.3 Theoretical description

In particle physics, the way of testing QFT predictions is by comparing it with quantities that can be measured in experiments; these are mainly *decay rates* Γ and *cross sections* σ. The same general procedure must be followed

in order to calculate both of these observables: determine all the relevant *Feynman Diagrams* to obtain the *amplitude* $\mathcal{M}$ of the process in question and apply *Fermi's Golden Rule* to obtain Γ or σ.

Feynman Diagrams contain the dynamical information about the process, while Fermi´s Golden Rule implies a phase space, which contains the kinematical information about the process [11].

In the following subsections a summary of Feynman rules for different interactions relevant for this work is presented.

2.3.1 Feynman rules for QED

Quantum Electrodynamics is the theory which couples charged spin-1/2 fields with a masless spin-1 field. The lagrangian of Quantum Electrodynamics is

$$\mathcal{L} = \mathcal{L}_0^{Dirac} + \mathcal{L}_0^{e.m.} + \mathcal{L}_1 \tag{2.3}$$

where

$$\mathcal{L}_0^{Dirac} = \bar{\psi}\left(\frac{i}{2}\gamma_\mu\overleftrightarrow{\partial}^\mu - m\right)\psi, \tag{2.4}$$

$$\mathcal{L}_0^{e.m.} = -\frac{1}{4}F_{\mu\nu}F^{\mu\nu} - \frac{1}{2}\zeta\left(\partial_\mu A^\mu\right)^2, \tag{2.5}$$

$$\mathcal{L}_1 = -g_e\bar{\psi}\gamma_\mu\psi A^\mu, \tag{2.6}$$

are the free Dirac lagrangian, the lagrangian of the Maxwell field and the interaction or coupling term, respectively, and the choice $\zeta = 0$ is the unitary gauge.

When an electromagnetic interaction is identified, the procedure to obtain the amplitude in momentum space is as follows [9, 11]:

1. Assign a momentum notation $p_1, p_2, ..., p_n$ to each *external line*, and $q_1, q_2, ..., q_n$ to each *internal line*, and draw an arrow indicating the direction of the momentum (not to confuse with the arrow on the line indicating whether the particle in question is a particle or an antiparticle).

	External Lines		Factor
	Spin 0 boson (or antiboson)		1
	Spin $\frac{1}{2}$ fermion (in, out)		$u, \bar{u}$
	Spin $\frac{1}{2}$ antifermion (in, out)		$v, \bar{v}$
	Spin 1 photon (in, out)		$\varepsilon_\mu, \varepsilon_\mu^*$
	Internal Lines – Propagators (need $+i\varepsilon$)		
	Spin 0 boson		$\dfrac{i}{p^2 - m^2}$
	Spin $\frac{1}{2}$ fermion		$\dfrac{i(\not{p} + m)}{p^2 - m^2}$
	Massive spin 1 boson		$\dfrac{-i\left(g_{\mu\nu} - p_\mu p_\nu / M^2\right)}{p^2 - M^2}$
	Massive spin 1 boson (Feynman Gauge)		$\dfrac{-i g_{\mu\nu}}{p^2}$

Figure 2.3: Summary of Feynman rules for QED [9].

- **Vertex factors**

Photon – spin 0 (charge $-e$) $i\,e\,(p + p')^\mu$

Photon – spin $\frac{1}{2}$ (charge $-e$) $i\,e\,\gamma^\mu$
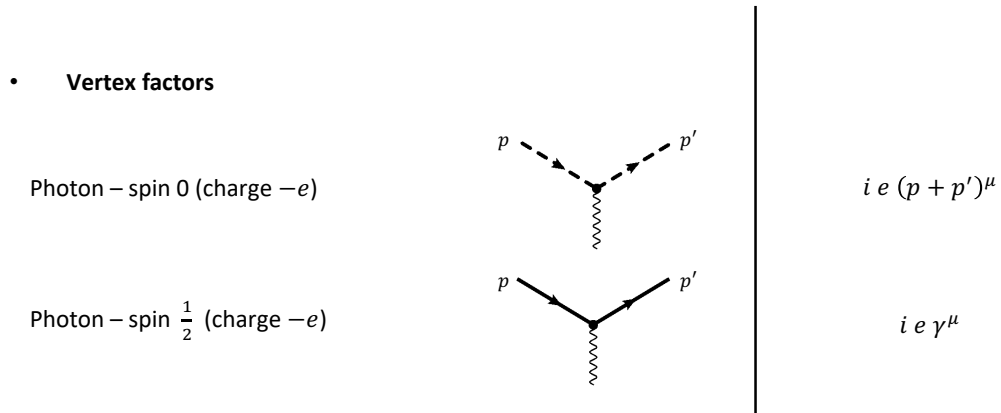
Figure 2.4: Vertex factors of QED [9].

2. Add a factor for each external and internal lines and vertex factors in accordance with Figure 2.3.

   Notice the parenthesis on internal lines - propagator in Figure 2.3 stating: (need $+i\epsilon$). This term ensures the propagator displaces the poles $p_0 = \pm E$ slightly bellow and above the axis, respectively.

3. Add a vertex factor as illustrated in Figure 2.4, where the coupling constant $g_e = \sqrt{4\pi\alpha}$.

4. For each vertex, a Dirac delta function must be included to ensure conservation of energy and momentum

$$(2\pi)^4 \delta^4(k_1 + k_2 + k_3), \tag{2.7}$$

   where k_1, k_2, k_3 are the four-momenta coming in or out of the vertex (for convention, four-momenta going out of the vertex must include a minus sign).

5. For each internal momentum q, write a factor

$$\frac{d^4q}{(2\pi)^4} \tag{2.8}$$

   and integrate.

18

6. Using the Dirac delta properties, group every delta until a single delta ensures overall conservation of energy and momentum

$$(2\pi)^4 \delta^4 (p_1 + p_2 + ... - p_n),$$ (2.9)

cancel this Dirac delta and multiply by a factor i. The final result is the amplitude $\mathcal{M}$.

Spinors u, v satisfy the momentum-space Dirac equations:

$$(\gamma^\mu p_\mu - m) u = 0$$ (2.10)

$$(\gamma^\mu p_\mu + m) v = 0.$$ (2.11)

Also they are orthogonal:

$$\bar{u}^{(1)} u^2 = 0$$ (2.12)

$$\bar{v}^{(1)} v^2 = 0,$$ (2.13)

and form a complete basis:

$$\sum_{s=1,2} u^{(s)} \bar{u}^{(s)} = (\gamma^\mu p_\mu + m)$$ (2.14)

$$\sum_{s=1,2} v^{(s)} \bar{v}^{(s)} = (\gamma^\mu p_\mu - m).$$ (2.15)

On the other hand, the polarization vectors $\epsilon_\mu^{(s)}$ with $s = 1, 2$ satisfy the momentum space Lorentz condition:

$$p^\mu \epsilon_\mu = 0.$$ (2.16)

They are orthogonal:

$$\epsilon_\mu^{(1)*} \epsilon^{(2)\mu} = 0,$$ (2.17)

normalized:

$$\epsilon^{\mu*} \epsilon_\mu = -1,$$ (2.18)

and obey the completeness relation:

19

$$\sum_{s=1,2} \epsilon_i^{(s)} \epsilon_j^{(s)*} = \delta_{ij}. \tag{2.19}$$

Once the amplitude $\mathcal{M}$ is obtained, the next step is to compute the cross section σ or the decay rate Γ. This final step is a kinematical procedure, which means every particular process will have their own cross section. For instance, if two particles in the initial state collide, producing n particles in the final state:

$$1 + 2 \rightarrow 3 + 4 + ... + n. \tag{2.20}$$

Then the standard notation for the differential scattering cross sections is given by (for further details, see [8]):

$$\begin{aligned} d\sigma = &\frac{(2\pi)^4 |\mathcal{M}|^2}{4\sqrt{(p_1 \cdot p_2)^2 - (m_1 m_2)^2}} \\ &\times d\Phi_n(p_1 + p_2; p_3, ..., p_{n+2}). \end{aligned} \tag{2.21}$$

The term $d\Phi_n$ is known as the *phase space*.

2.3.2 Effective theories and Vector Meson Dominance (VMD) model

The Standard Model has shown to be one of the most precise theories in physics, giving astounding theoretical predictions. Hadrons are made up of quarks and hence hadron interactions should be mediated by the strong, weak and electromagnetic interactions of the quarks they are made of. However, at low energies they can be though of as constituent particles, *i.e.* the interactions occur at hadronic level, neglecting the quark interactions. This is the main idea of an *Effective Theory* of the strong interaction.
Back in 1960 before the development of the Standard Model and QCD, J.J. Sakurai proposed in his paper *"Theory of strong interactions"* [12] the existence of vector mesons coupled to the electromagnetic current, by the hadronic isospin and hypercharge currents using the idea of a Yang-Mills theory from 1954. Nowadays these tools are used in what is known as *Vector Meson Dominance (VMD)* [10]; where vectorial mesons can be recognized as *"Dynamical gauge bosons of hidden local symmetry"* in the framework of a

low-energy effective Lagrangian of masless two-flavored QCD, thus arriving at Sakurai's massive Yang-Mills Lagrangian [13].

The effective lagrangian that couples vector mesons with the electromagnetic field (photons) was given by Kroll, Lee and Zumino in 1967 [14]:

$$\mathcal{L}'_{mix} = \frac{e' m_V^2}{f_V} V'_\mu A'^\mu - \frac{1}{2} \left(\frac{e'}{f_V} \right)^2 m_V^2 V'^2_\mu \tag{2.22}$$

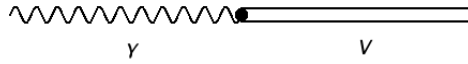The Feynman diagram coupling a photon with a neutral vector meson is illustrated in Figure 2.5

Figure 2.5: Coupling of a photon γ with a neutral vector meson V (ρ, ω).

The coupling term is given by the coefficient from Equation (2.22), which, just for notation, here is presented as $\frac{e\, m_V^2}{g_V}$.

Vector mesons $V = (\rho, \omega)$ are electrically neutral, this would imply an impossibility of electromagnetic interaction with a photon γ, nevertheless, their constituent quarks $(q\bar{q})$ are not, this is what makes the interaction possible. As mentioned earlier, at low energies (≤ 1 GeV [10]), the interaction of mesons is described by vector dominance, and even though this is just an effective theory, has great phenomenological and experimental support [10, 13]. The regime of QCD that deals with low energies is known as *confinement*, because quarks are confined within a certain region (hadrons). As seen from the vector dominance point of view, the strong interaction is only responsible for this quark packaging, not the hadron interaction itself, and of course, as the energy increases, this effective theory will no longer be valid.

Chapter 3

Symmetries

According to *Emmy Noether* [15], symmetries play an important role in particle physics; there's a direct relation between symmetries and conservation laws in physics.

This chapter begins with *Noether's Theorem* and the existence of conserved currents, followed by a summary of spontaneous symmetry breaking, Goldstone theorem and two direct applications of it; the σ model and soft pion theorems.

Next, a detailed exposition of anomalies in QFT is presented: *Anomalous Ward Identities* (AWI) and how they allow the process $\pi^0 \to \gamma\gamma$. The chapter ends with the *Wess-Zumino-Witten* (WZW) anomaly action. This chapter follows the same procedure as that in *Reinhold* [16] and *Cheng and Li* [17] books.

3.1 Noether's theorem

There are two types of symmetries: *discrete* and *continuous*. For instance, rotating a circle around its center creates a continuous symmetry, because it doesn't matter the angle of rotation, the circle will remain the same, whereas a square has only four angles of rotation around the center that leave the shape unchanged. The former creates a continuous spectrum of angles, whereas the latter creates a discrete spectrum.

Noether's theorem states that for every system described by a *Lagrangian*

$$L = \int d^3x \mathcal{L}\left(\phi_i(x), \partial_\mu \phi_i(x)\right), \tag{3.1}$$

which has an equation of motion given by:

$$\partial_\mu \frac{\delta \mathcal{L}}{\delta(\partial_\mu \phi_i)} - \frac{\delta \mathcal{L}}{\delta \phi_i} = 0 \tag{3.2}$$

any *continuous* symmetry transformation that leaves the action $S = \int L \, dt$ invariant will imply the existence of a *conserved current*

$$\partial^\mu J_\mu(x) = 0 \tag{3.3}$$

where a *charge Q* will be defined by the temporal component of the current:

$$Q(t) = \int d^3x \, J_0(x) \tag{3.4}$$

and will be a constant of motion

$$\frac{dQ}{dt} = 0. \tag{3.5}$$

This section has summarized Noether's theorem. Next section introduces the spontaneous symmetry breaking and the Goldstone theorem.

3.2 Spontaneous symmetry breaking and the Goldstone theorem

In the last section it was mentioned how Noether's theorem relates conservation laws to symmetries in the Lagrangian. For instance, the U(1) symmetry leaves the Lagrangian $\mathcal{L} = \mathcal{L}(\varphi, \partial_\mu \varphi)$ invariant under the symmetry

$$\varphi(x) \rightarrow \varphi'(x) = e^{-i\theta} \varphi(x) \tag{3.6}$$

If the variable θ does not depend on the spacetime coordinates x, then the lagrangian has a *global symmetry*. On the other hand, if it does depend on the spacetime coordinates $\theta(x)$, then the lagrangian has a *local symmetry*. Global and local symmetries are important in quantum field theory because global symmetries represent quantities that cannot be measured, while local symmetries represent physical quantities that are conserved *locally* (like charge and lepton number). Local symmetries preserve *causality* as postulated by special relativity, *i.e.*, they guarantee those physical quantities can't travel faster than the speed of light.

23

There are some systems with their own symmetries that have a *ground state*, and sometimes these ground states do not satisfy the same symmetries as the original system. When this happens, it is said the system has a *Spontaneous Symmetry Breaking*. The most popular shape for this topic is the so-called mexican hat. If a little marble sits on top of the mexican hat, it has an unstable ground state, because any perturbation on any direction will cause the marble to roll down. In other words, the perturbation has broken the symmetry, because now the marble finds itself at a minimum potential energy, different from the ground state (the top of the hat).

Nambu (1960) and Goldstone (1962) found out that the spontaneous breakdown of a continuous symmetry implies the existence of masless spinless particles. These scalar particles are known as *Nambu-Goldstone bosons* or just *Goldstone bosons* [18, 19].

As seen in Equation 3.3, continuous symmetries of the Lagrangian imply the existence of conserved currents, and charges are constants of motion (Equation 3.5), however, with symmetry breakdown, $Q(t)$ will not be well defined. The transformation of a generic field operator $\phi(x)$ will have the form:

$$
\begin{aligned}
\phi(x) \to \phi^{'}(x) &= e^{i\epsilon Q}\phi(x)e^{-i\epsilon Q} \\
&= \phi(x) + i\epsilon[Q, \phi(x)] + ...
\end{aligned}
\tag{3.7}
$$

Current conservation (Equation 3.3) implies that:

$$
\begin{aligned}
0 &= \int d^3x[\partial^\mu J_\mu(\mathbf{x}, t), \phi(0)] \\
&= \partial^0 \int d^3x[J^0(\mathbf{x}, t), \phi(0)] + \int d\mathbf{S} \cdot [\mathbf{J}(\mathbf{x}, t), \phi(0)].
\end{aligned}
\tag{3.8}
$$

Considering an infinite surface, the second term on the right hand side vanishes, and hence

$$
\frac{d}{dt}[Q(t), \phi(0)] = 0.
\tag{3.9}
$$

If this conmutator has a non-vanishing vacuum expectation value

$$
\langle 0|[Q(t), \phi(0)|0\rangle \equiv \eta \neq 0,
\tag{3.10}
$$

then the symmetry is spontaneously broken. Inserting a complete set of states, Equation (3.10) can be written as

$$\sum_n (2\pi)^3 \delta^3(\mathbf{p}_n) \, \langle 0|J_0(0)|n\rangle \, \langle n|\phi(0)|0\rangle \, e^{-iE_n t}$$

$$- \langle 0|\phi(0)|n\rangle \, \langle 0|J_0|0\rangle \, e^{iE_n t} = \eta. \tag{3.11}$$

This expression can only be satisfied if there exist an intermediate state where $E_n = 0$ for $\mathbf{p}_n = 0$. This massless state is the *Goldstone boson*, with the property that:

$$\langle n|\phi(0)|0\rangle \neq 0$$
$$\langle 0|J_0(0)|n\rangle \neq 0 \tag{3.12}$$

meaning the Goldstone boson can be conected to vacuum by the current $J_0(0)$ or by the operator $\phi(0)$.

3.2.1 The $SU(2)_L \times SU(2)_R$ σ model

The σ model (Schwinger, Polkinghorne, Gell-Mann and Levy) illustrates the ideas of spontaneous symmetry breaking and Goldstone bosons. Consider the following fields: isotriplet of pions $\boldsymbol{\pi} = (\pi_1, \pi_2, \pi_3)$, an isoscalar σ field and an isodoublet of nucleons $N = (p, n)$. The Lagrangian is given by

$$\mathcal{L} = \frac{1}{2}[(\partial_\mu \sigma)^2 + (\partial_\mu \boldsymbol{\pi})^2] + \bar{N}i\gamma^\mu \partial_\mu N$$
$$+ g\bar{N}(\sigma + i\boldsymbol{\tau} \cdot \boldsymbol{\pi}\gamma_5)N - V(\sigma^2 + \boldsymbol{\pi}^2) \tag{3.13}$$

where $\boldsymbol{\tau}$ are the Pauli matrices, and

$$V(\sigma^2 + \boldsymbol{\pi}^2) = \frac{-\mu^2}{2}(\sigma^2 + \boldsymbol{\pi}^2) + \frac{\lambda}{4}(\sigma^2 + \boldsymbol{\pi}^2)^2. \tag{3.14}$$

This lagrangian will have two symmetries: the first one is under the $SU(2)$ transformation:

$$\sigma \to \sigma' = \sigma$$
$$\boldsymbol{\pi} \to \boldsymbol{\pi}' = \boldsymbol{\pi} + \boldsymbol{\alpha} \times \boldsymbol{\pi} \tag{3.15}$$
$$N \to N' = N - i\boldsymbol{\alpha} \cdot \frac{\boldsymbol{\tau}}{2}N,$$

with the $SU(2)$ generators

$$Q^a = \int J_0^a(x)d^3x. \tag{3.16}$$

The second symmetry is given by the *axial $SU(2)$* transformation

$$\sigma \to \sigma' = \sigma + \boldsymbol{\beta} \cdot \boldsymbol{\pi}$$
$$\boldsymbol{\pi} \to \boldsymbol{\pi}' = \boldsymbol{\pi} - \boldsymbol{\beta}\sigma \tag{3.17}$$
$$N \to N' = N + i\boldsymbol{\beta} \cdot \frac{\boldsymbol{\tau}}{2}\gamma_5 N,$$

with the axial charges or generators

$$Q^{5a} = \int A_0^a(x)d^3x. \tag{3.18}$$

Generators from Equations 3.16 and 3.18 generate (for the sake of redundancy) what's called the $SU(2)_L \times SU(2)_R$ *algebra.*
If one chooses $\mu^2 > 0$, $\langle 0|\boldsymbol{\pi}|0\rangle = 0$ and

$$\langle 0|\sigma|0\rangle = \nu, \tag{3.19}$$

then it is found that $\boldsymbol{\pi}$'s are the Goldstone bosons. The choice of letting the σ field take the spontaneous symmetry breaking term implies that axial charges Q^{5a} do not annihilate the vacuum, that is

$$\langle 0|A_\mu^a(0)|\pi^a\rangle \neq 0 \tag{3.20}$$

In consecuence, the $SU(2)_L \times SU(2)_R$ symmetry is broken spontaneously into the $SU(2)$ symmetry generated by the charges from Equation 3.16.

3.3 PCAC and soft pion theorems

3.3.1 Soft pion theorems

As introduced in spontaneous symmetry breaking, particles will only realize the portion of the symmetry which is also respected by the ground state. It turns out that electromagnetic and weak currents are generated by an $SU(3)_R \times SU(3)_L$ algebra, and their symmetries need to be broken in such a way that their vacuum is only $SU(3)$ symmetric (just like the σ model).

Goldstone theorem implies that there are eight massless pseudoscalar mesons associated with the broken axial charges $Q^{5a}, a = 1, ..., 8$.

But in reality, those pseudoscalar mesons correspond to the octet of mesons $\boldsymbol{\pi}, \boldsymbol{K}, \eta$ (Figure 2.2). Since these mesons are non massless, the $SU(3)_R \times SU(3)_L$ symmetry needs also to be broken explicitly in order to introduce these mass terms. This is achieved by a *chiral symmetry breaking*

$$\mathcal{H} = \mathcal{H}_0 + \lambda\mathcal{H}' \tag{3.21}$$

where $\mathcal{H}_0$ respects the $SU(3)_L \times SU(3)_R$ symmetry, but $\mathcal{H}'$ does not.

Lastly, taking advantage of the fact that pion isotriplet is much lighter than $K's$ and $\eta's$, the $\lambda\mathcal{H}'$ term can be further decomposed in

$$\lambda\mathcal{H}' = \lambda_1\mathcal{H}_1 + \lambda_2\mathcal{H}_2 \tag{3.22}$$

where $\mathcal{H}_1$ is $SU(2)_L \times SU(2)_R$ invariant, and $\lambda_1 >> \lambda_2$.

By doing this, the $\lambda_2\mathcal{H}_2$ term is associated with the pion mass, *i.e.*, in the *chiral symmetry* limit ($\lambda_2 = 0$), pions will be taken to be massless particles. This is known as a *soft pion theorem*.

3.3.2 PCAC

From Equation 3.20 it is clear that there is a coupling relation between Goldstone bosons $\pi^a(x)$ with *broken* axial charges Q^{5a} and currents A_μ^a when there is spontaneous symmetry breaking. This can be re-written as

$$\langle 0|A_\mu^a(0)|\pi^b(p)\rangle = if^{ab}p_\mu \qquad a, b = 1, 2, 3 \tag{3.23}$$

Assuming the SU(2) isospin symmetry is broken, the constant f^{ab} can be written as

$$f^{ab} = f_\pi\delta^{ab} \tag{3.24}$$

where f_π is the pion decay constant, which has been measured experimentally in $\pi^+ \to l^+ + \nu_l$, obtaining $f_\pi \approx 93MeV$ [17]. Taking the divergence of the axial vector current and using the fact that $p^2 = m^2$

$$\langle 0|\partial^\mu A_\mu^a(0)|\pi^b(p)\rangle = \delta^{ab}f_\pi m_\pi^2 \tag{3.25}$$

and it is clear how, if $\lambda_2 = 0$ in Equation 3.22 (chiral limit), the $SU(2)_L \times SU(2)_R$ symmetry is exact, and the axial current is conserved

$$\partial^\mu A_\mu^a = 0, \tag{3.26}$$

which, from Equation 3.25 implies that $m_\pi^2 = 0$ (Goldstone boson).
However, if $\lambda_2 \neq 0$ (that is, if the symmetry is explicitly broken) then Equation 3.25 can be rewritten as

$$\langle 0|\partial^\mu A_\mu^a(0)|\pi^b(p)\rangle = f_\pi m_\pi^2 \langle 0|\phi^a(0)|\pi^b(p)\rangle, \tag{3.27}$$

where ϕ^a is the pion field operator. Comparing both sides, it's clear the relation

$$\partial^\mu A_\mu^a = f_\pi m_\pi^2 \phi^a \qquad a = 1, 2, 3 \tag{3.28}$$

This generalization of the axial current conservation is known as the *partially conserved axial-vector current* **PCAC** hypotesis, (Nambu, Chou, Gell-Mann and Levy).

3.3.3   Low energy theorems with one soft pion

Equation 3.28 implies the non-conservation of the axial vector current. This hypothesis leads to physical implications, like the *Goldberger-Treiman relation*, which couples two nucleon states $p(k'), n(k)$ with one axial vector current $\langle p(k')|A_\mu^1 + iA_\mu^2|n(k)\rangle$.
After Lorentz covariance, applying the current divergence and comparing terms, this matrix element gives the relation

$$\frac{2f_\pi m_\pi^2}{-q^2 + m_\pi^2} g_{\pi NN}(q^2) = 2m_N g_A(q^2) + q^2 h_A(q^2) \tag{3.29}$$

where $g_{\pi NN}(q^2)$ is the πNN coupling constant, $q = k - k'$, g_A, h_A are form factors and m_N is the mass of the nucleons.
Setting $q^2 = 0$, that is, at low energies, then

$$f_\pi g_{\pi NN}(0) = m_N g_A(0). \tag{3.30}$$

Assuming the transition from $q^2 = 0$ to $q^2 = m_\pi^2$ is a smooth function, then

$$g_{\pi NN}(0) \approx g_{\pi NN}(m_\pi^2) = g_{\pi NN} \tag{3.31}$$

Equation 3.32 becomes the *Goldberger-Treiman relation*

$$f_\pi g_{\pi NN} = m_N g_A(0). \tag{3.32}$$

Several assumptions have been made during this process, being the transition from $q^2 = 0$ to $q^2 = m_\pi^2$ the most relevant. The justification of this is that among the hadronic scale, π's are the lightest, and as a consequence, Goldberger-Treiman relation is believed to cause only small errors on experimental results because of this assumption.

3.4   Anomalies in QFT

3.4.1   Conserved currents

Returning to the lagrangian of QED from Chapter 2, this time written in the form

$$\mathcal{L}_{QED} = \bar{\psi}(i\slashed{\partial} - m + e\slashed{A})\psi - \frac{1}{4}F_{\mu\nu}F^{\mu\nu}, \tag{3.33}$$

defining the following currents

$$
\begin{aligned}
vector & \quad j_\mu = \bar{\psi}\gamma_\mu\psi \\
axial & \quad j_\mu^5 = \bar{\psi}\gamma_\mu\gamma_5\psi \\
pseudoscalar & \quad P = \bar{\psi}\gamma_5\psi,
\end{aligned} \tag{3.34}
$$

using Dirac equation $(i\slashed{\partial} - m + e\slashed{A})\psi = 0$ and the anticommutation relation $\{\gamma_5, \gamma_\mu\} = 0$ the following conservation laws are stablished

$$\partial^\mu j_\mu = 0 \tag{3.35}$$

$$\partial^\mu j_\mu^5 = 2imP. \tag{3.36}$$

Vector current is naturally conserved, and axial current will be only conserved for masless fermions

$$\partial^\mu j_\mu^5 = 0. \tag{3.37}$$

3.4.2   Ward identities and the anomaly

Consider the expectation value of the time-ordered product of a current j^μ with some generic operators O^i (also known as Green function)

$$\langle 0|Tj^\mu(x)O^1(y_1)...O^n(y_n)|0\rangle \tag{3.38}$$

Differentiating this expression gives

$$\partial_\mu^x \langle 0|Tj^\mu(x)O^1(y_1)...O^n(y_n)|0\rangle =$$
$$\langle 0|T\partial_\mu^x j^\mu(x)O^1(y_1)...O^n(y_n)|0\rangle$$
$$+\sum_{i=1}^n \langle 0|T[j^0(x),O^i(y_i)]\delta(x_0 - y_{i0})O^1...O^{i-1}O^{i+1}...O^n)|0\rangle \tag{3.39}$$

where

$$T[A(t_1)B(t_2)] = \Theta(t_1 - t_2)A_{t_1}B_{t_2} + \Theta(t_2 - t_1)B_{t_2}A_{t_1}. \tag{3.40}$$

Once the conservation law $\partial_\mu^x j^\mu(x)$ and the commutation relations $[j^0(x),O^i(y_i)]$ are inserted, Equation 3.39 is known as the **Ward Identity**.
For instance, for a 3-point function defined by the Green function

$$\tau^\mu(x,y,z) = \langle 0|Tj^\mu(z)\psi(x)\bar\psi(y)|0\rangle \tag{3.41}$$

using the equal-time commutator

$$[j^0(z),\psi(x)]\delta(z_0 - x_0) = -\psi(z)\delta^4(z - x)$$
$$[j^0(z),\bar\psi(y)]\delta(z_0 - y_0) = \bar\psi(z)\delta^4(z - y) \tag{3.42}$$

and the vector current conservation 3.35, then, Equation 3.39 transforms in what is known as the Vector Ward Identity in x-space

$$\partial_\mu^z \tau^\mu(x,y,z) = - \langle 0|T\psi(z)\bar\psi(y)|0\rangle \, \delta^4(z - x) + \langle 0|T\psi(x)\bar\psi(z)|0\rangle \, \delta^4(z - y)$$
$$= -iS_F(z - y)\delta^4(z - x) + iS_F(x - z)\delta^4(z - y). \tag{3.43}$$

Analogously, the 3-point function given by the Green function

$$\langle 0|Tj_\mu(x)j_\nu(y)j_\lambda^5(z)|0\rangle \tag{3.44}$$

which after applying the covariant derivative in momentum space has the form

$$q^\lambda T_{\mu\nu\lambda} = \int d^4x d^4y d^4z e^{ik_1 x + ik_2 y - iqz}$$
$$\cdot \langle 0|T j_\mu(x) j_\nu(y) \partial_z^\lambda j_\lambda^5(z)|0\rangle \tag{3.45}$$

and using the conservation law 3.36 (commutation relations vanishes) gives rise to the **Axial Ward Identity**

$$q^\lambda T_{\mu\nu\lambda} = 2im \int d^4x d^4y d^4z e^{ik_1 x + ik_2 y - iqz}$$
$$\cdot \langle 0|T j_\mu(x) j_\nu(y) P(z)|0\rangle \tag{3.46}$$
$$= 2m T_{\mu\nu}.$$

Vector Ward Identity can be expressed in momentum space as well

$$k^\mu T_{\mu\nu\lambda} = k^\nu T_{\mu\nu\lambda} = 0. \tag{3.47}$$

The amplitudes $T_{\mu\nu\lambda}$ and $T_{\mu\nu}$ will be obtained via Feynman rules for some triangle diagrams, and it turns out that when inserting them into Equations 3.46 and 3.47, they will *violate* Ward Identities. An additional term, the **"anomaly"** occurs.

3.4.3 Triangle graphs

Naturally, one question arises: which Ward identity will be violated? It turns out if the Vector Ward Identity (VWI) is fullfilled, then the Axial Ward Identity (AWI) is anomalous, or vice-versa. This last means an anomalous term will always exist.

When performing the integral from Equation 3.45, a surface term appears, causing the anomalous term to take place. To illustrate this, consider the amplitudes of *triangle graphs* from Figure 3.1.

Applying Feynman rules, the correspondent amplitudes in momentum space are

$$T_{\mu\nu\lambda} = i \int \frac{d^4p}{(2\pi)^4} (-) \operatorname{tr} \frac{i}{\not{p} - m} \gamma_\lambda \gamma_5 \frac{i}{\not{p} - \not{q} - m} \gamma_\nu \frac{i}{\not{p} - \not{k}_1 - m} \gamma_\mu$$
$$+ \begin{pmatrix} k_1 \longleftrightarrow k_2 \\ \mu \longleftrightarrow \nu \end{pmatrix} \tag{3.48}$$
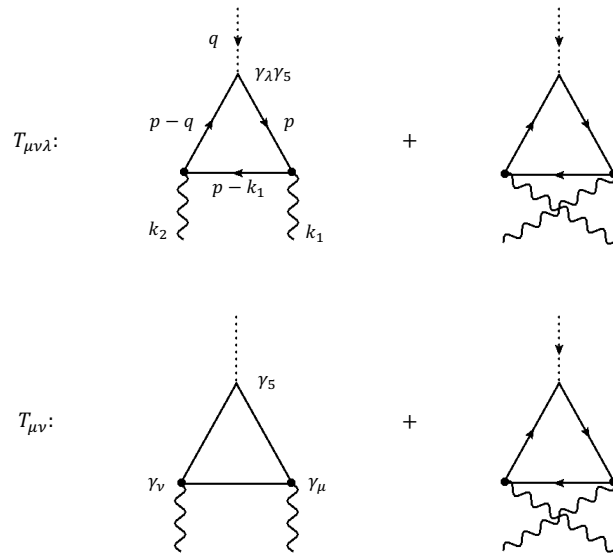
Figure 3.1: Triangle graphs with vector-vector axial currents (up) and vector-vector-pseudoscalar currents (down) [16].

$$T_{\mu\nu} = i \int \frac{d^4p}{(2\pi)^4}(-)\,\text{tr}\,\frac{i}{\not{p}-m}\gamma_5\frac{i}{\not{p}-\not{q}-m}\gamma_\nu\frac{i}{\not{p}-\not{k}_1-m}\gamma_\mu$$
$$+ \begin{pmatrix} k_1 \longleftrightarrow k_2 \\ \mu \longleftrightarrow \nu \end{pmatrix} \tag{3.49}$$

where $q = k_1 + k_2$, and of course, the slash notation $\not{p} = \gamma^\mu p_\mu$. These two amplitudes can be related with AWI (Equation 3.46) as follows

$$q^\lambda T_{\mu\nu\lambda} = 2m T_{\mu\nu} + R^1_{\mu\nu} + R^2_{\mu\nu} \tag{3.50}$$

where

$$R^1_{\mu\nu} = \int \frac{d^4p}{(2\pi)^4}\,\text{tr}\left[\frac{1}{\not{p}-\not{k}_2-m}\gamma_5\gamma_\nu\frac{1}{\not{p}-\not{q}-m}\gamma_\mu\right.$$
$$\left.-\frac{1}{\not{p}-m}\gamma_5\gamma_\nu\frac{1}{\not{p}-\not{k}_1-m}\gamma_\mu\right] \tag{3.51}$$

$$R^2_{\mu\nu} = \int \frac{d^4p}{(2\pi)^4}\,\text{tr}\left[\frac{1}{\not{p}-\not{k}_2-m}\gamma_5\gamma_\nu\frac{1}{\not{p}-\not{q}-m}\gamma_\mu\right.$$
$$\left.-\frac{1}{\not{p}-m}\gamma_5\gamma_\nu\frac{1}{\not{p}-\not{k}_1-m}\gamma_\mu\right] \tag{3.52}$$

If $R^1, R^2 \to 0$, then the AWI is satisfied. This can be accomplished by shifting the integral variable $p \to p + k_2$ in Equation 3.51 and $p \to p + k_1$ in Equation 3.52, however, both integrals are *linearly divergent*, which, from definition, forbids the variable shifting.

3.4.4 Anomalous terms

Given an integral of the form

$$\Delta(a) = \int_{-\infty}^{\infty} dx[f(x+a) - f(x)]$$
$$= \int_{-\infty}^{\infty} dx[af'(x) + \frac{a^2}{2!}f''(x) + ...] \tag{3.53}$$
$$= a[f(\infty) - f(-\infty)] + \frac{a^2}{2!}[f'(\infty) - f'(-\infty)]$$

if the integral converges, then $f(\pm\infty) = f'(\pm\infty) = f''(\pm\infty) = ... = 0$ and it's clear how $\Delta(a) = 0$, therefore the shifting variable $x \to x - a$ can be done.

However, if the integral is linearly divergent, then, in general, $f(\pm\infty) \neq 0, f'(\pm\infty) = f''(\pm\infty) = ... = 0$, which, from Equation 3.53, implies a non-vanishing surface term

$$\Delta(a) = a[f(\infty) - f(-\infty)] \neq 0. \tag{3.54}$$

Generalizing this integral to 4-dimensional Minkovsky space and aplying Gauss theorem, the surface term is

$$\Delta(a) = i2\pi^2 a^\mu \lim_{R\to\infty} R_\mu R^2 f(R) \tag{3.55}$$

This result can be used to calculate Equations 3.51 and 3.52, which after some trace identities will give

$$R^1_{\mu\nu} = -\frac{1}{8\pi^2}\varepsilon_{\mu\nu\alpha\beta}k_1^\alpha k_2^\beta \tag{3.56}$$

$$R^2_{\mu\nu} = -\frac{1}{8\pi^2}\varepsilon_{\mu\nu\alpha\beta}k_1^\alpha k_2^\beta. \tag{3.57}$$

Therefore, the AWI ends up with the following anomalous form

$$q^\lambda T_{\mu\nu\lambda} = 2mT_{\mu\nu} - \frac{1}{4\pi^2}\varepsilon_{\mu\nu\alpha\beta}k_1^\alpha k_2^\beta. \tag{3.58}$$

Finally, Equation 3.58 is quite a general result in the sense that the internal momentum p could be shifted by some amount and the integral would be altered.

This argument can be regularized by shifting the internal momentum

$$p \to p + a \tag{3.59}$$

where

$$a = \alpha k_1 + (\alpha - \beta)k_2. \tag{3.60}$$

By doing this, Equation 3.58 will end up in what's known as the **anomalous AWI** (for $\beta \neq 1$)

$$q^{\lambda}T_{\mu\nu\lambda}(\beta) = 2mT_{\mu\nu} - \frac{1-\beta}{4\pi^2}\varepsilon_{\mu\nu\alpha\beta}k_1^{\alpha}k_2^{\beta}. \tag{3.61}$$

The exact same procedure can be applied to VWI (Equation 3.47) to get the **anomalous VWI** (for $\beta \neq 1$)

$$k_1^{\mu}T_{\mu\nu\lambda}(\beta) = \frac{1+\beta}{8\pi^2}\varepsilon_{\nu\lambda\alpha\beta}k_1^{\alpha}k_2^{\beta}. \tag{3.62}$$

With these definitions, there is no value of β such that both the anomalous AWI (Equation 3.61) and the anomalous VWI (Equation 3.62) can be fullfilled, as mentioned before.

1. *VWI and anomalous AWI*

   $\beta = -1$ causes the VWI to be fullfilled (Equation 3.47) and the anomalous AWI takes the form

   $$q^{\lambda}T_{\mu\nu\lambda} = 2mT_{\mu\nu} + \mathcal{A}_{\mu\nu} \tag{3.63}$$

   where the term

   $$\mathcal{A}_{\mu\nu} = -\frac{1}{2\pi^2}\varepsilon_{\mu\nu\alpha\beta}k_1^{\alpha}k_2^{\beta} \tag{3.64}$$

   is known as the **ABJ anomaly** (Adler-Bell-Jackiw) in momentum space.

2. *Anomalous VWI and AWI*

   $\beta = 1$ causes the AWI to be fullfilled (Equation 3.46) and the anomalous VWI takes the form

   $$k_1^{\mu}T_{\mu\nu\lambda} = -\frac{1}{2}\mathcal{A}_{\nu\lambda} \tag{3.65}$$

3. *Anomalous AWI and anomalous VWI*

   If $\beta = 1/3$ the anomaly will be equally distributed between the AWI and VWI

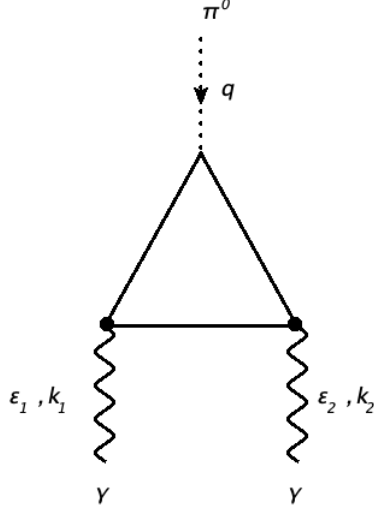 $$k_1^{\mu}T_{\mu\nu\lambda} = -\frac{1}{3}\mathcal{A}_{\nu\lambda} \tag{3.66}$$

Figure 3.2: Triangle graph of neutral pion decay into two photons $\pi^0 \rightarrow \gamma\gamma$,
where the loop is composed of quarks [16].

$$q^\lambda T_{\mu\nu\lambda} = 2m T_{\mu\nu} + \frac{1}{3}\mathcal{A}_{\mu\nu} \tag{3.67}$$

Finally, Adler-Bardeen theorem ensures the anomaly will receive no radiative corrections in higher order perturbation theory.

3.5 Decay $\pi^0 \rightarrow \gamma\gamma$

One application of ABJ anomaly can be found on the neutral pion decay into two photons $\pi^0 \rightarrow \gamma\gamma$, illustrated in Figure 3.2. Historically, this decay led to the discovery of the anomaly.
The transition matrix element is given by

$$
\begin{aligned}
\langle \gamma(\varepsilon_1, k_1), \gamma(\varepsilon_2, k_2)| \left|\pi^0(q)\right\rangle \\
= (2\pi)^4 \delta^4(q - k_1 - k_2)\varepsilon_1^\mu(k_1)\varepsilon_2^\nu(k_2)\Gamma_{\mu\nu}(k_1, k_2, q)
\end{aligned}
\tag{3.68}
$$

where

$$\Gamma_{\mu\nu} = e^2 i \int d^4x d^4y e^{ik_1 x + ik_2 y} \left\langle 0\left|T j_\mu x j_\nu y\right|\pi^0(q)\right\rangle. \tag{3.69}$$

36

As introduced in Chapter 2, pion is a pseudoscalar (Figure 2.2) with negative parity (0^-), this property causes the amplitude 3.69 to be a pseudotensor with a general Lorentz structure

$$\Gamma_{\mu\nu}(k_1, k_2, q) = \Gamma(q^2)\varepsilon_{\mu\nu\alpha\beta}k_1^\alpha k_2^\beta \tag{3.70}$$

Equation 3.69 can be reduced with what's known as the **LSZ reduction formula** (Lehmnan, Symanzik, Zimmermann) [16]

$$
\begin{aligned}
\Gamma_{\mu\nu} = e^2\left(-q^2 + m_\pi^2\right) \int d^4y d^4z e^{ik_2 y - iqz} \\
\cdot \langle 0|T\phi_\pi(z)j_\nu(y)j_\mu(0)|0\rangle
\end{aligned}
\tag{3.71}
$$

Comparing Equations 3.71 and 3.45 (after x transformation with energy-momentum conservation), it can be concluded that the pion field couples to the non-conserved axial currents.

Substituting PCAC relation 3.28 ($\partial^\lambda j_\lambda^{5a} = f_\pi m_\pi^2 \phi^a(z)$) into Equation 3.71 gives

$$q^\lambda T_{\mu\nu\lambda} = \frac{f_\pi m_\pi^2}{e^2(-q^2 + m_\pi^2)}\Gamma_{\mu\nu} \tag{3.72}$$

this last expression contains no poles in the limit $q \to 0$, meaning there are no physical values between the pion and the vacuum, therefore left hand side has to vanish as $q \to 0$. This means the right hand side of Equation 3.70 must vanish too

$$\Gamma(q^2 = 0) = 0 \tag{3.73}$$

which means pion should not decay into photons, however, pion decay has been observed in nature. This is known as the **Sutherland-Veltman paradox**, and it's resolved by the anomaly.

By modifying PCAC (in the presence of gauge fields), Equation 3.72 transforms into

$$q^\lambda T_{\mu\nu\lambda} = \frac{f_\pi m_\pi^2}{e^2(-q^2 + m_\pi^2)}\Gamma_{\mu\nu} - \frac{c}{2\pi^2}\varepsilon_{\mu\nu\alpha\beta}k_1^\alpha k_2^\beta \tag{3.74}$$

The numerical value of c is determined from the quark model

$$c = 3 \cdot \frac{1}{2}\operatorname{tr}\left[\{Q, Q\}\frac{\lambda^3}{2}\right] = 3 \cdot \frac{1}{6} = \frac{1}{2} \tag{3.75}$$

where

$$Q = \frac{1}{3} \begin{pmatrix} 2 & 0 & 0 \\ 0 & -1 & 0 \\ 0 & 0 & -1 \end{pmatrix}, \qquad \lambda^3 = \frac{1}{2} \begin{pmatrix} 2 & 0 & 0 \\ 0 & -1 & 0 \\ 0 & 0 & -1 \end{pmatrix} \qquad (3.76)$$

and the factor of 3 accounts for the quark colour degrees of freedom.
Now, in the limit $q \to 0$ in Equation 3.74 (soft pion limit)

$$\lim_{q \to 0} \Gamma_{\mu\nu}(k_1, k_2, q) = \frac{e^2 c}{2\pi^2 f_\pi} \varepsilon_{\mu\nu\alpha\beta} k_1^\alpha k_2^\beta \qquad (3.77)$$

and comparing Equations 3.77 and 3.70

$$\Gamma(q^2 = 0) = \frac{e^2 c}{2\pi^2 f_\pi}. \qquad (3.78)$$

This expression can be used to obtain the decay rate Γ (Chapter 2) integrating over phase space, summing over photon polarization and substituting numerical values

$$\Gamma(\pi^0 \to \gamma\gamma) = 7.63 \text{ GeV} \qquad (3.79)$$

which is in agreement with the experimental value (see references [8, 16])

$$\Gamma_{exp}(\pi^0 \to \gamma\gamma) = 7.37 \pm 1.5 \text{ GeV}. \qquad (3.80)$$

In conclusion, pion decay $\pi^0 \to \gamma\gamma$ is only possible because of the anomaly, and it also serves as an evidence of the colour degrees of freedom of quarks.

3.6 Wess-Zumino-Witten (WZW) anomaly action

Decay $\pi^0 \to \gamma\gamma$ introduced in Section 3.5 includes the triangle-graph loop composed of quarks (Figure 3.5), meaning the couplings are between quarks-photon and pion-quarks.
A direct coupling between neutral pion and two photons is not possible, because π^0 is uncharged, and uncharged particles do not experience the electromagnetic interaction, which is the only interaction photons γ can experience. Nevertheless, a low-energy effective theory can couple neutral pions with photons, making a first-order neutral pion decay into two photons possible.

Such effective theory is given by the *Wess-Zumino-Witten (WZW)* anomaly action, first proposed by Julius Wess and Bruno Zumino [20] and later adjusted by Edward Witten [21].

Although the WZW anomaly action is a more general low-energy effective theory coupling mesons to themselves and to gauge fields, the particular case of pions coupling to photons is given by the effective lagrangian [10]

$$\mathcal{L}_A = \frac{N_c}{48\pi^2}\epsilon^{\mu\nu\alpha\beta}[e\,A_\mu \operatorname{Tr}(QL_\nu L_\alpha L_\beta + QR_\nu R_\alpha R_\beta - i\,e^2 F_{\mu\nu}A_\alpha T_\beta)] \quad (3.81)$$

with

$$
\begin{aligned}
&L_\mu \equiv U\partial_\mu U^\dagger, \qquad R_\mu \equiv \partial_\mu U U^\dagger, \\
&T_\beta = \operatorname{Tr}(Q^2 L_\beta + Q^2 R_\beta + \frac{1}{2}QUQU^\dagger L_\beta + \frac{1}{2}QU^\dagger QU R_\beta)
\end{aligned}
\quad (3.82)
$$

where A_μ is the photon field, $F_{\mu\nu}$ is the photon field strenght $N_c = 3$ is the number of colors, and the quantity $U = \exp(i\,\boldsymbol{\tau}\cdot\boldsymbol{\pi}'/\nu)$ is related to the pion field. Expanding to first order in the pion field, Equation 3.81 transforms into

$$\mathcal{L}_A = \frac{\alpha N_c}{24\pi f_\pi}\epsilon^{\mu\nu\alpha\beta}F_{\mu\nu}F_{\alpha\beta}\,\pi^0 \quad (3.83)$$

where f_π is the pion form factor given in Equation 3.24. This effective lagrangian shows a clear coupling between neutral pion field π^0 and two photons $F_{\mu\nu}\,F_{\alpha\beta}$ at first order.

Throughout this chapter, a detailed demonstration of the Anomalous Ward Identities (AWI) has been presented, whose existence allows the decay process $\pi^0 \to \gamma\gamma$ with a theoretical decay rate $\Gamma = 7.63$ GeV (Equation 3.79). This result will be used in the following chapters.

Finally, the Wess-Zumino-Witten (WZW) anomaly action has been introduced for the particular case of the pion coupling to two photons. This general structure (Equation 3.83) will appear later on this work for every pion decay process.

Chapter 4

Resonant states

In this chapter, the definition of resonant particles is introduced along with the definition of *mean lifetime* τ and *decay width* Γ. Then, a detailed calculation of the propagator of unstable particles (complex mass scheme) is presented. The chapter ends with an exposition of the Higgs decay $H \to \gamma\gamma$, and a discussion on how it is related with the decay process $\pi^0 \to \gamma\gamma$.

4.1 Resonant particles

Aside from the proton, whose decay has not been observed experimentally, the neutron whose lifetime can last up to 15 minutes [8], as well as the photon and the electron, particle lifetimes come in a wide range, from 10^{-6} s to 10^{-23} s. This value relies on the type of decay; strong, weak or electromagnetic. Particles with short lifetimes have only enough time to travel short distances before they decay, for instance, a particle traveling at the speed of light with a lifetime of 10^{-23}s can travel up to 3×10^{-15} m.

These distances are so small that they cannot be detected with current detectors, instead, ultra-short lived particles appear as *resonant states* from interactions of longer-lived particles.

Figure 4.1 shows resonant states from scattering process $e^+e^- \to hadrons$. When initial electron and positron interact, they can scatter elastically ($e^+e^- \to e^+e^-$), or they could produce two photons ($e^+e^- \to \gamma\gamma$), or, with enough energy, produce two muons (or taus) ($e^+e^- \to \mu^+\mu^-$), or they could produce a pair of quarks ($e^+e^- \to q\bar{q}$). When this last process occurs, final state quarks interact (via strong interaction) creating an entire cascade of quarks,

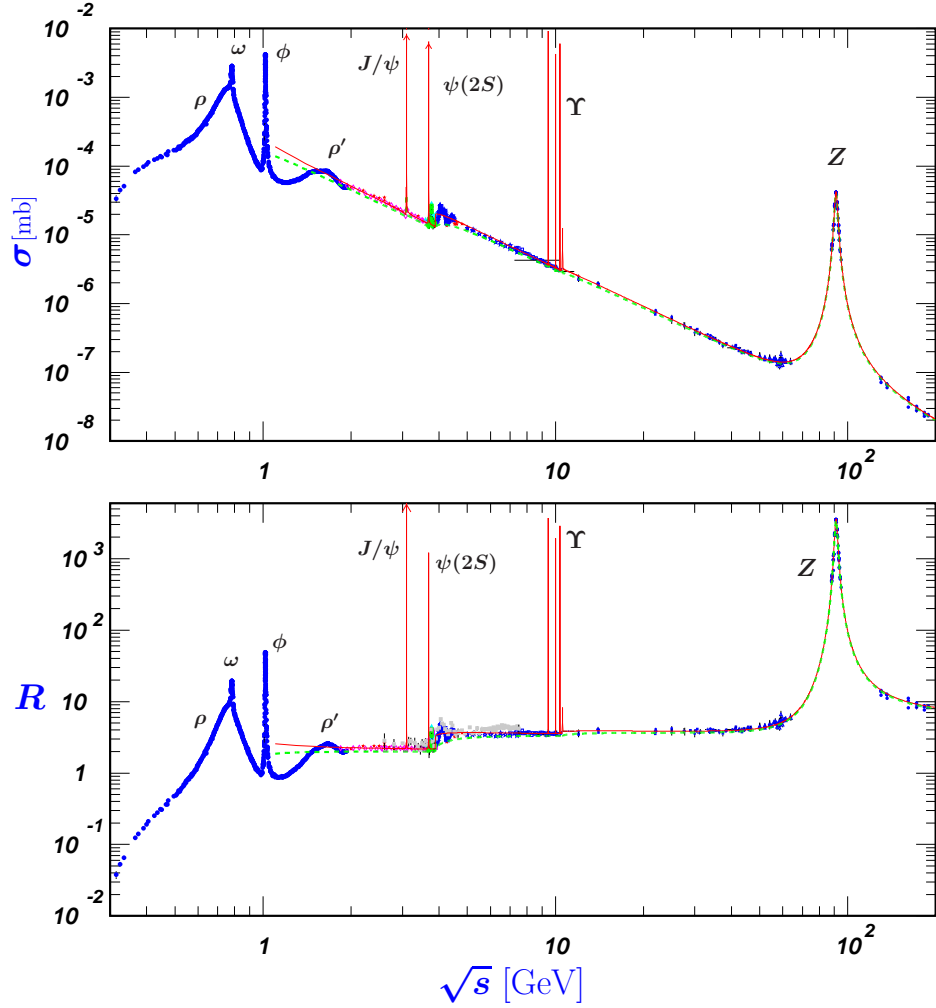Figure 4.1: Resonant states from scattering process $e^+e^- \to hadrons$. Horizontal axis corresponds to center-of-mass energy, vertical axis corresponds to cross section (up) and ratio $R(s) = \sigma(e^+e^- \to hadrons, s)/\sigma(e^+e^- \to \mu^+\mu^-, s)$ (down) [8].

41

antiquarks and gluons, which create all the kinds of mesons and baryons introduced in Chapter 2. What is observed in Figure 4.1 is the process $e^+e^- \to hadrons$.

Resonances appear as virtual particles, and decay to other particles via electromagnetic, weak, or strong interaction (VMS introduced in Chapter 2 is an effective theory used to explain mesons decay).

Lifetime of these intermediate particles can be estimated with the mean lifetime formula.

$$\tau = \frac{\hbar}{\Gamma} \tag{4.1}$$

where the *decay width* Γ is measured at half-maximum of the corresponding resonance peak.

4.2 Propagator of unstable particles

Unlike stable particles, properties like mass m and width Γ of unstable particles have a different nature [22, 23, 24], which is reflected on their propagator.

Breit-Wigner expression for vector propagator

$$D_{\mu\nu}^V(q^2) = \frac{-g_{\mu\nu} + \frac{q_\mu q_\nu}{M_V^2}}{q^2 - M_V^2 + iM_V\Gamma_V} \tag{4.2}$$

doesn't satisfy electromagnetic Ward identity [25]. In this section, the proper structure of vector propagator for unstable particles used in this work will be deduced.

Beginning with the structure of the propagator for the case of scalar particles

$$\begin{aligned} D(q) &= i \int_{s_0}^{\infty} \frac{\rho(m^2)dm^2}{q^2 - m^2 + i\epsilon} \\ &= i \int_{s_0}^{\infty} D_0(q^2, m^2)\rho(m^2)dm^2 \end{aligned} \tag{4.3}$$

where $\rho(m^2)$ is called the spectral function, $D_0(q^2, m^2)$ is the "bare" scalar propagator and s_0 is a parameter to be determined.

This expression contains a pole at $q^2 \to s_0$. Using the integration rule

$$\int_a^b \frac{f(x)dx}{x \pm i\epsilon} = \mp i\pi f(0) + PV \int_a^b \frac{f(x)}{x}dx \tag{4.4}$$

where $PV \int_a^b$ stands for Cauchy's Principal Value of the integral. Using Equation 4.4, then Equation 4.3 takes the form

$$D(q) = -i\pi\rho(q^2) + PV \int \frac{\rho(m^2)}{q^2 - m^2}dm^2 \tag{4.5}$$

Setting the left hand side of Equation 4.5 to the Breit-Wigner scalar propagator

$$D^{BW}(q) = \frac{1}{q^2 - M^2 + iM\Gamma} \tag{4.6}$$

then, the spectral function $\rho(q^2)$ is revealed as

$$-\pi\rho(q^2) = \frac{-M\Gamma}{(q^2 - M^2)^2 + M^2\Gamma^2} \tag{4.7}$$

Setting $q^2 = m^2$ gives the form $\rho(m^2)$

$$\rho(m^2) = \frac{1}{\pi} \frac{M\Gamma}{(m^2 - M^2)^2 + M^2\Gamma^2} \tag{4.8}$$

In the calculation of Equation 4.5 the limits of integration $(-\infty < m^2 < \infty)$ are calculated when doing the same identification of terms with Equation 4.4, this means $s_0 = -\infty$.

To define the structure of vector propagator, it is necessary to assume the spectral function $\rho(m^2)$ 4.8 is the same for both vectorial and scalar propagators, then, from Equations 4.2 and 4.8

$$D_{\mu\nu}(q) = \frac{1}{\pi} \int_{-\infty}^{+\infty} \frac{-g_{\mu\nu} + q_\mu q_\nu/(m^2 - i\epsilon)}{q^2 - m^2 + i\epsilon} \frac{M\Gamma dm^2}{[m^2 - M^2]^2 + M^2\Gamma^2} \tag{4.9}$$

Using the method of contour integration along the lower contour C_- and a change of variable gives

$$\begin{aligned} D_{\mu\nu}(q) &= -\frac{M\Gamma}{\pi} \oint_{C_-} \frac{(g_{\mu\nu} - q_\mu q_\nu/(z - i\epsilon))\,dz}{(z - z_-)(z - z_+)(z - z_0)} \\ &= \frac{-g_{\mu\nu} + q_\mu q_\nu/(M^2 - iM\Gamma)}{q^2 - M^2 + iM\Gamma} \end{aligned} \tag{4.10}$$

where $z_0 = q^2 + i\epsilon$ and $z_\pm = M^2 \pm iM\Gamma$. Defining the vectorial propagator with a universal complex mass squared

$$D_{\mu\nu}(q) = \frac{-g_{\mu\nu} + q_\mu q_\nu / M_P^2}{q^2 - M_P^2} \qquad (4.11)$$

where $M_P^2 = M^2 - iM\Gamma$ (known as the complex mass scheme) gives the modified version of vector propagator 4.2 that satisfies the electromagnetic Ward identity.

This "dressed" propagator can be obtained by the substitution $M_0 - i\epsilon \rightarrow M^2 - iM\Gamma$. So, the infinitesimal value ϵ which is used as a mathematical tool to go around the pole in bare propagator, is an analog of the decay width in this new framework.

In the main calculations of this work, this will be the form of the vector propagator, and one of the specific objectives is to explore the effects of the decay width in the observables under consideration.

4.3   Higgs decay

This section presents the Higgs decay to illustrate the importance of the unstable features of intermediate states. Namely of the W and Z gauge bosons.

Higgs boson is a neutral particle of spin-0 (scalar) proposed by Peter Higgs, Robert Brout, François Englert, Gerald Guralnik, C. R. Hagen, and Tom Kibble in 1964. Its discovery in 2013 at CERN has been crucial for the standard model, because it confirms that the *Higgs mechanism* is what gives mass to quarks, leptons, and W and Z bosons in the context of local gauge theory.

Figure 4.2 shows the main decays of the Higgs boson near the region of the mass $M_H = 125$ GeV. As can be seen, $b\bar{b}$ is the dominant decay, followed by WW, gg, $\tau\tau$, $c\bar{c}$, ZZ, $\gamma\gamma$ and so on. Before the discovery of the Higgs particle, two of the most promising channels of a light Higgs were $H \rightarrow \gamma\gamma$ (at one-loop) and $H \rightarrow ZZ^* \rightarrow l\bar{l}l\bar{l}$. Despite the smallness of their branching ratios (0.23% and 0.012%, respectively), they enjoy clean signatures and lower backgrounds with respect to other channels, *i.e.*, final state particles can be measured very precisely [26, 27, 28, 8].

Higgs decay $H \rightarrow \gamma\gamma$ is dominated by top quark loop and W boson loop as shown in Figure 4.3, while the decay $H \rightarrow ZZ^* \rightarrow l\bar{l}l\bar{l}$ is illustrated in Figure
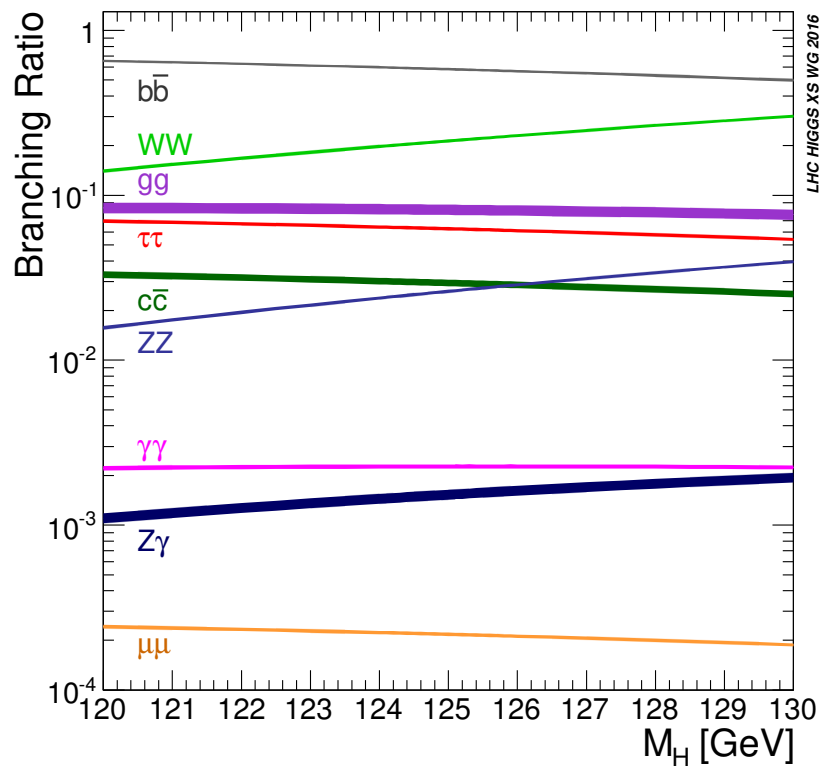
Figure 4.2: Branching ratios (vertical axis) of the main decays of the Higgs boson near the Higgs mass $M_H = 125$ GeV (horizontal axis) [8].
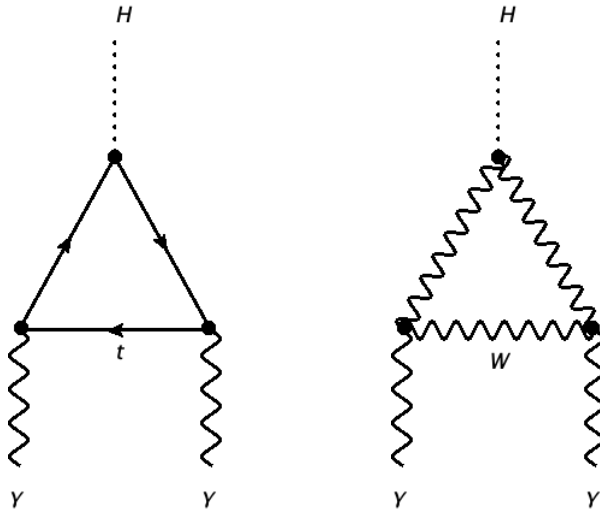
Figure 4.3: Higgs decay $H \to \gamma\gamma$ mediated by top loop (left) and W loop (right).

4.4 (right). In both of these channels, the Higgs particle can be produced via proton-proton scattering, where each proton interacts with the emission of one gluon. By doing this, the Higgs can be reconstructed as a resonance. Historically, this is the way the Higgs particle was discovered and its mass m_H was measured (Figure 4.5).

Its decay width Γ_H has been recently determined via the enhancement produced when both of the gauge bosons W, Z are on-shell, but at that energy, the Higgs particle is off-shell [29].

Another channel where the Higgs can be created is $pp \to H \to W^+W^- \to l^+l^-\nu\bar{\nu}$, illustrated in Figure 4.4 (left), however, this is not distinguishable from the process $pp \to W^+W^- \to l^+l^-\nu\bar{\nu}$, and both processes involve neutrinos as final particles, which are not easily measured in experiments.

At such energy, at least one of the gauge bosons is off-shell ($M_W \sim 80\,\text{MeV}$, $M_Z \sim 90\,\text{MeV}$)

The next chapter will explore analog effects, while exploring the on-shell and off-shell regions for the ρ and ω mesons in $\rho - \omega - \pi$ interactions as part of intermediate processes.
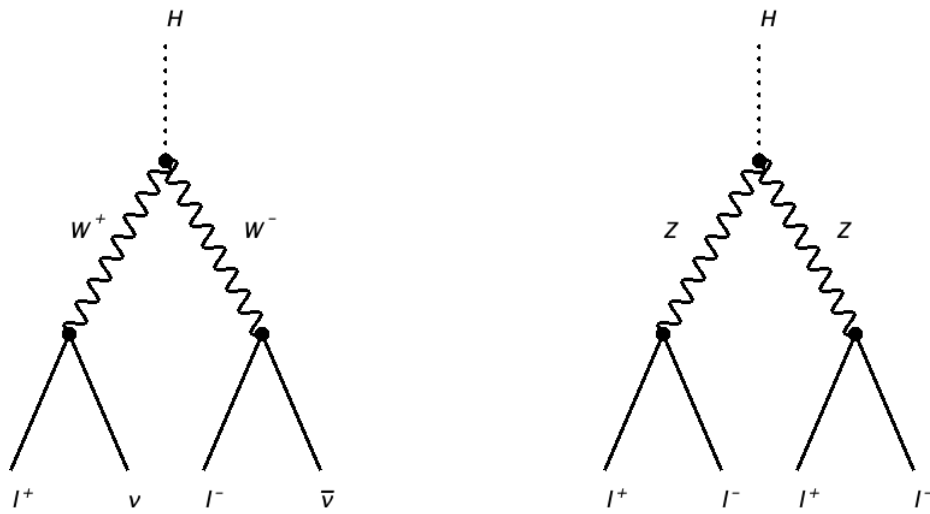
Figure 4.4: Higgs decay $H \to W^+W^- \to l^+l^-\nu\bar{\nu}$ (left) and $H \to ZZ \to l\bar{l}l\bar{l}$ (right).
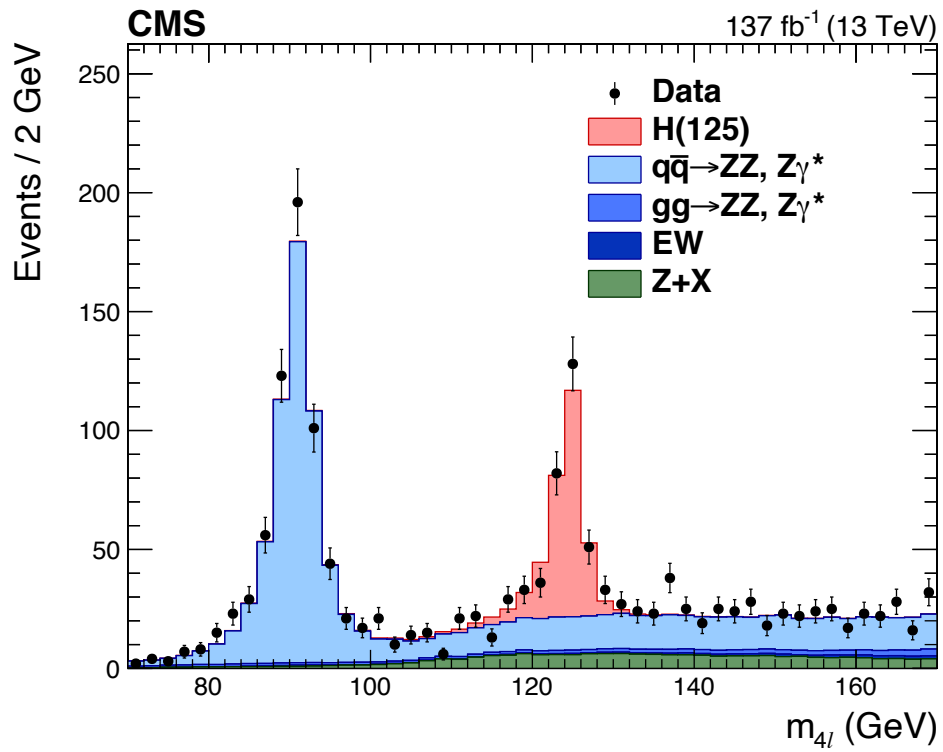
Figure 4.5: Results from CMS run 2 showing the mass distribution of two Z bosons in four leptons event. Blue region shows the expected distribution from ZZ* production, while red region is the Higgs boson signal [8].

Chapter 5

1-Loop correction to the $\rho\omega\pi$ vertex

The theoretical calculation of this thesis begins in this chapter. First, the amplitude of pion decay $\pi^0 \to \gamma\gamma$ with intermediate resonant states ρ, ω is obtained, then the exact same decay with 1-loop correction $\rho\omega\pi$. By comparing both amplitudes, an expression for the effective coupling constant $g_{\rho\omega\pi}(q^2)$ is obtained. Generalizing the final state photons condition, is possible to use this last expression on a particular scattering process to be exposed in the next chapter.

5.1 Pion decay $\pi^0 \to \gamma\gamma$ with intermediate resonant states ρ^0, ω^0

As introduced in Section 4.1, quarks interact via strong interaction (for the sake of redundancy) and create final state mesons. Such phenomenon occurs in processes like the pion decay $\pi^0 \to \gamma\gamma$, as seen in Section 3.5. This process is driven by the WZW anomaly discussed in Section 3.6. Note that the strong interaction among quarks was not incorporated, instead, the strong interaction effects are incorporated by considering that the quarks hadronize into two vector mesons before producing the two final-state photons. Thus, the $\rho\omega\pi$ coupling can be directly linked to the anomaly. Henceforth, this is how this simplification will be referred to indistinctly.

The case study of this work is the particular scenario where those quarks hadronize into vectorial mesons ρ^0 and ω^0 (because of conservation of angular
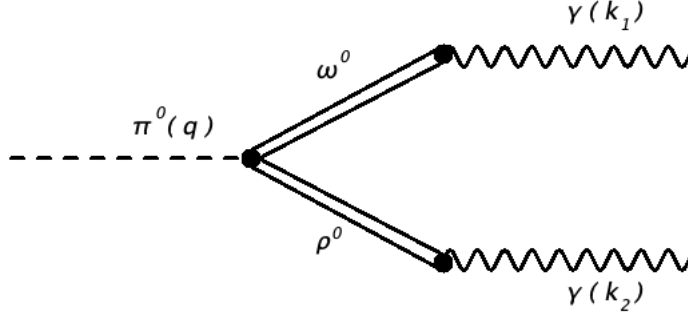
Figure 5.1: Pion decay $\pi^0 \to \gamma\gamma$ with intermediate resonant states ω^0, ρ^0

momentum) from Section 2.2.2 and end up decaying into photons via VMD model (Section 2.3.2). The Feynman diagram of this process is illustrated in Figure 5.1

Using the VMD effective lagrangian (Equation 2.22), the amplitude is given by

$$
\begin{aligned}
i\mathcal{M}^{(0)} =& ig_{\rho\omega\pi}\varepsilon^{\theta\tau\mu\lambda}k_1^\theta k_2^\tau D_\rho^{\mu\nu}(k_1)D_\omega^{\chi\lambda}(k_2)\left(-i\frac{e\,m_\rho^2}{g_\rho}g_{\nu\alpha}\right) \\
&\cdot \left(-i\frac{e\,m_\omega^2}{g_\omega}g_{\chi\beta}\right)\epsilon_\alpha^*(k_1)\epsilon_\beta^*(k_2)
\end{aligned}
\tag{5.1}
$$

where $g_{\rho\omega\pi}$ is the *effective coupling constant* from the $\rho\omega\pi$ vertex, $\varepsilon^{\theta\tau\mu\lambda}$ is the Levi-Civita tensor, q, k_1, k_2 are the four-momentum from pion and final state on-shell photons, respectively, $\epsilon_\alpha^*(k_1), \epsilon_\beta^*(k_2)$ are the polarization vectors from each photon, and the term

$$
D_{\rho,\omega}^{\mu\nu}(k) = i\left(\frac{-g^{\mu\nu} + \frac{k^\mu k^\nu}{m_{\rho,\omega}^2 - i\,m_{\rho,\omega}\Gamma_{\rho,\omega}}}{k^2 - m_{\rho,\omega}^2 + i\,m_{\rho,\omega}\Gamma_{\rho,\omega}}\right)
\tag{5.2}
$$

is the propagator of unstable particles from Section 4.2. Substituting Equation 5.2 into the amplitude 5.1, it gives

50

$$
\begin{aligned}
i\mathcal{M}^{(0)} =& ig_{\rho\omega\pi}\varepsilon^{\theta\tau\mu\lambda}k_1^\theta k_2^\tau \left(i\frac{-g^{\mu\nu} + \frac{k_1^\mu k_1^\nu}{m_\rho^2 - i\,m_\rho\Gamma_\rho}}{k_1^2 - m_\rho^2 + i\,m_\rho\Gamma_\rho} \right) \cdot \\
& \cdot \left(i\frac{-g^{\chi\lambda} + \frac{k_2^\chi k_2^\lambda}{m_\omega^2 - i\,m_\omega\Gamma_\omega}}{k_2^2 - m_\omega^2 + i\,m_\omega\Gamma_\omega} \right) \left(-i\frac{e\,m_\rho^2}{g_\rho}g_{\nu\alpha} \right) \cdot \\
& \cdot \left(-i\frac{e\,m_\omega^2}{g_\omega}g_{\chi\beta} \right) \epsilon_\alpha^*(k_1)\epsilon_\beta^*(k_2)
\end{aligned}
\tag{5.3}
$$

After squaring this amplitude and summing over polarization states (see Appendix 8.1), Equation 5.3 gives

$$
|\mathcal{M}^{(0)}|^2 = g_{\rho\omega\pi}^2 \left(\frac{16\pi^2\alpha^2 m_\pi^4}{g_\rho^2 g_\omega^2} \right).
\tag{5.4}
$$

Next step is to obtain the decay rate Γ (Section 2.3.1). This process is a two-body decay and, according to PDG rev. on kinematics [8]

$$
\begin{aligned}
d\Gamma &= \frac{1}{32\pi^2}|\mathcal{M}^{(0)}|^2\frac{|\mathbf{p}_1|}{M^2}d\Omega \\
|\mathbf{p}_1| &= |\mathbf{p}_2| = \frac{1}{2M}\sqrt{\lambda(M^2, m_1^2, m_2^2)}
\end{aligned}
\tag{5.5}
$$

where $\mathbf{p}_1$ and $\mathbf{p}_2$ are the three-momentum of final state particles 1 and 2 (both final photons), M, m_1, m_2 are the masses of initial particle and final particles, respectively, $d\Omega = d\phi_1 d(cos\theta_1)$ is the solid angle of particle 1 and $\lambda(a, b, c) = a^2 + b^2 + c^2 - 2ab - 2ac - 2bc$ is the Källén function. After integration and replacing values (see Appendix 8.2), the decay rate becomes

$$
\Gamma = \frac{1}{16\pi}\frac{|\mathcal{M}^{(0)}|^2}{m_\pi}
\tag{5.6}
$$

Inserting Equation 5.4 into Equation 5.6 gives the theoretical decay rate

$$
\Gamma = g_{\rho\omega\pi}^2\frac{\alpha^2\pi\,m_\pi^3}{g_\rho^2 g_\omega^2}
\tag{5.7}
$$

The value of the decay rate can be obtained from experimental results using Equation 4.1 as follows. First, solving for the total decay width Γ_T and using pion mean life $\tau = 8.43 \times 10^{-17}$ s and $\hbar = 6.582 \times 10^{-22}$ MeV $\cdot$ s
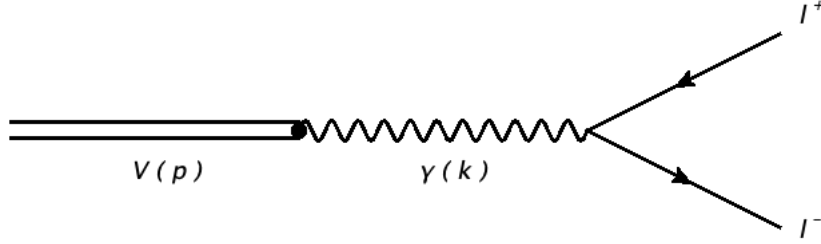
51

Figure 5.2: Process $V \to l^+l^-$, where $V = \rho^0, \omega^0$ and $l^\pm = e^\pm, \mu^\pm$

$$\Gamma_T = \frac{\hbar}{\tau} = \frac{6.582 \times 10^{-22} \text{ MeV} \cdot \text{s}}{8.43 \times 10^{-17} \text{ s}} = 7.8078 \times 10^{-6} \text{ MeV}. \tag{5.8}$$

Then, from [8], the pion decay mode $\pi^0 \to \gamma\gamma$ has a branching ratio B.R. = 98.823%, this means

$$\Gamma_{exp}(\pi^0 \to \gamma\gamma) = \text{B.R.} \cdot \Gamma_T = 7.7159 \times 10^{-6} \text{ MeV} \tag{5.9}$$

Comparing Equations 5.9 and 5.7 gives an expression for $g_{\rho\omega\pi}$

$$g_{\rho\omega\pi} = \left(\frac{g_\rho^2 g_\omega^2}{\alpha^2 m_\pi^3 \pi} \right)^{\frac{1}{2}} \times (7.7159 \times 10^{-9} \text{ GeV}). \tag{5.10}$$

Constants g_ρ and g_ω are obtained from $V \to l^+l^-$ processes like the one illustrated in Figure 5.2 using the VMD approach. They can be obtained from (see reference [30])

$$g_V = \sqrt{\frac{4\pi\alpha^2}{3\Gamma_V m_V^2}(2m_l^2 + m_V^2)\sqrt{(m_V^2 - 4m_l^2)}} \tag{5.11}$$

where Γ_V stands for the experimental decay width of vectorial mesons $V = \rho^0, \omega^0$ and l could be an electron e^- or a muon μ^- (see Tables 2.1 and 2.4 for the numerical values). This gives the dimensionless constants

$$\begin{aligned} g_\rho &= 4.9869, \\ g_\omega &= 16.5129. \end{aligned} \tag{5.12}$$

Substituting them into Equation 5.10 gives the final expression

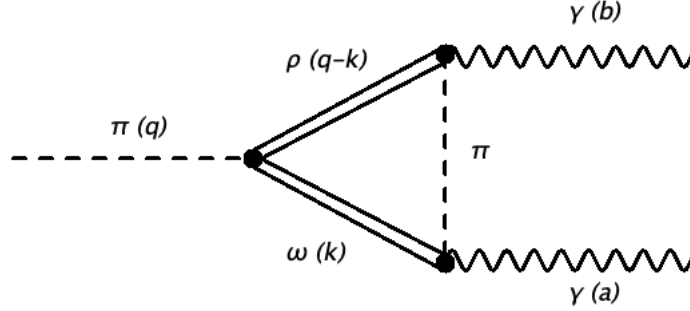$$g_{\rho\omega\pi} = 11.2746 \text{ GeV}^{-1} \tag{5.13}$$

Figure 5.3: Re-scattering correction of pion decay $\pi^0 \to \gamma\gamma$ with intermediate resonant states ρ, ω, π

An extended analysis [31] considering more observables gives

$$g_{\rho\omega\pi} = 11.712 \text{ GeV}^{-1} \tag{5.14}$$

5.2 Re-scattering process $\pi^0 \to \gamma\gamma$ with intermediate loop $\rho\omega\pi$

A higher-order correction of $\pi^0 \to \gamma\gamma$ consist of a triangle graph like the ones introduced in section 3.4.3. This time, the intermediate resonant states ρ, ω, π create a loop (again, omitting the neutral exponent for the sake of notation). This kind of correction will be referred to as *"re-scattering"*, illustrated in Figure 5.3 (including its symmetric part). The four-vector k stands for the internal momentum running inside the loop. Applying Feynman rules (omitting a global i term) gives the amplitude

$$\mathcal{M}^{(1)} = -\int \frac{d^4 k}{(2\pi)^4} g_{\rho\omega\pi} \, g_{\omega\pi\gamma} \, g_{\rho\gamma\pi} \varepsilon^{\mu\nu\theta\tau}(a+b)_\theta \, k_\tau D^\omega_{\nu\lambda}(k)\cdot$$
$$\cdot \, \varepsilon^{\lambda\eta\phi\delta} k_\pi a_\delta D^\pi(a-k) \varepsilon^{\alpha\beta\chi\Lambda}(a+b-k)_\chi b_\Lambda \cdot \tag{5.15}$$
$$\cdot \, D^\rho_{\mu\alpha}(a+b-k) + \begin{pmatrix} a \longleftrightarrow b \\ \eta \longleftrightarrow \beta \end{pmatrix}$$

This time, pion propagator D^π is the one of a spin-0 boson (see Figure 2.3), four momenta q, a, b are the pion and final state photons (which, unlike the ones from Section 5.1, this time can be both on-shell $\gamma\gamma$, both off-shell $\gamma^*\gamma^*$

53

or a combination on-shell off-shell $\gamma\gamma^*$), coupling constants $g_{\omega\pi\gamma}, g_{\rho\pi\gamma}$ are obtained from VMD model

$$
\begin{aligned}
g_{\rho\pi\gamma} &= g_{\rho\omega\pi}\frac{e}{g_\omega}, \\
g_{\omega\pi\gamma} &= g_{\rho\omega\pi}\frac{e}{g_\rho},
\end{aligned}
\tag{5.16}
$$

and the last term in Equation 5.15 indicates the crossed term with the interchange of the corresponding index and four vectors.

Taking coupling constants out of the integral, Equation 5.15 factorizes as

$$
\mathcal{M}^{(1)} = \frac{e^2 g_{\rho\omega\pi}^3}{g_\rho g_\omega} G_{loop}.
\tag{5.17}
$$

Computer software *Mathematica* [32] and *Package-X* [33] have been used to calculate G_{loop} based on dimensional regularization (excluding coupling constants). However, software limitations (complex integration) have forced the propagators to omit its complex term $im_V\Gamma_V$. By the time of writing this work, a complete calculation which includes that complex term is being developed with *LoopTools* [34].

In the meantime, a little mathematical trick has been elaborated to explore how the final results are aligned with or without this complex term.

5.2.1 Stable states

Computing the case where the complex term $im_V\Gamma_V$ is omitted (as well as global i terms), and both photons are on-shell, G_{loop} transforms into:

$$
\begin{aligned}
G_{loop}^R = -\int & \frac{d^4k}{(2\pi)^4}\varepsilon^{\mu\nu\theta\tau}(a+b)_\theta\, k_\tau \left(\frac{-g^{\nu\lambda} + \frac{k^\nu k^\lambda}{m_\omega^2}}{k^2 - m_\omega^2}\right) \cdot \\
& \cdot \varepsilon^{\lambda\eta\phi\delta}k_\pi a_\delta \left(\frac{1}{(a-k)^2 - m_\pi^2}\right)\varepsilon^{\alpha\beta\chi\Lambda}(a+b-k)_\chi b_\Lambda \cdot \\
& \cdot \left(\frac{-g^{\mu\alpha} + \frac{(a+b-k)^\mu(a+b-k)^\alpha}{m_\rho^2}}{(a+b-k)^2 - m_\rho^2}\right) + \begin{pmatrix} a \longleftrightarrow b \\ \eta \longleftrightarrow \beta \end{pmatrix}
\end{aligned}
\tag{5.18}
$$

Following *Package-X* documentation [33] for computing loop integrals (this includes multiplying by an overall factor of $\frac{i}{16\pi^2}$ and adding the constant -

$\gamma_E + \ln(4\pi)$ to every $\frac{1}{\epsilon}$ pole, where γ_E is the Euler-Mascheroni constant) and using the initial conditions ($a \cdot a = b \cdot b = 0$, $q \cdot q = q^2$, $q = a + b$, $a \cdot q = b \cdot q = a \cdot b = \frac{1}{2}q^2$), gives a long expression (not written here, but latter it will be plotted) in terms of pion momentum q^2 to be compared with the complex integral. It's important to remark how the initial condition $q \cdot q = q^2$ indicates how the pion is not on-shell in general.

The divergent term $\frac{1}{\epsilon}$ is neglected, considering this term should be cancelled by counter-terms, while the μ^2 term is a cutoff term, which is taken at $1\,\text{GeV}$, as discussed in Section 2.3.2.

5.2.2 Unstable states

As mentioned before, *Package-X* [33] does not allow to introduce complex terms in the propagator's denominator. A mathematical trick has been used to include the imaginary part in the denominator

$$m_V^2 \to \sqrt{m_V^4 + (m_V \Gamma_V)^2} \qquad (5.19)$$

By replacing it, the squared mass *absorbs* the decay width Γ_V. Of course this is not a complete description of the integral, however, comparing G_{loop}^R and G_{loop}^C gives a good idea of how related both approaches are.

Figure 5.5 shows both results squared and divided by q^2 just for normalization. These plots match so identically that is hard to distinguish between them, proving how similar both descriptions are.

5.2.3 On-shell, off-shell photons condition

If one of the two final-state photons is off-shell ($\pi^0 \to \gamma\gamma^*$) the initial conditions change as ($a \cdot a = m_a^2$, $b \cdot b = 0$, $q \cdot q = q^2$, $q = a + b$, $a \cdot q = \frac{1}{2}(q^2 + m_a^2)$, $b \cdot q = \frac{1}{2}(q^2 - m_a^2)$, $a \cdot b = \frac{1}{2}(q^2 - m_a^2)$) then G_{loop} will be a function of two variables: m_a^2, q^2. This result is illustrated in Figure 5.5. A non-allowed kinematical region is visible in the middle of this surface, which corresponds to the points where $q^2 = m_a^2$, causing the loop contribution to diverge.

Regions of interest for this particular scenario occur at $m_a^2 = m_\pi^2, m_\rho^2, m_\omega^2$ (Figure 5.6), because each propagator's denominator value will decrease, causing the loop contribution to diverge. Further discussion on this will be exposed in Chapter 6.
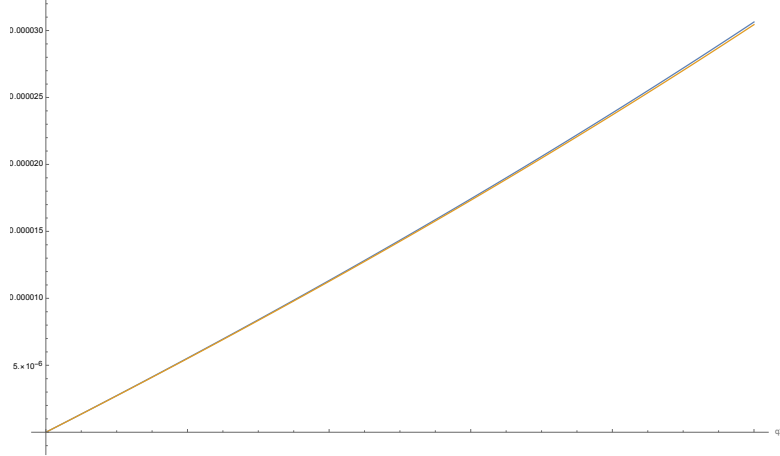
Figure 5.4: $|G^R_{loop}|^2/q^2$ (blue) and $|G^C_{loop}|^2/q^2$ (orange). Horizontal axis corresponds to q^2. Both graphs are so similar they appear to be superimposed.
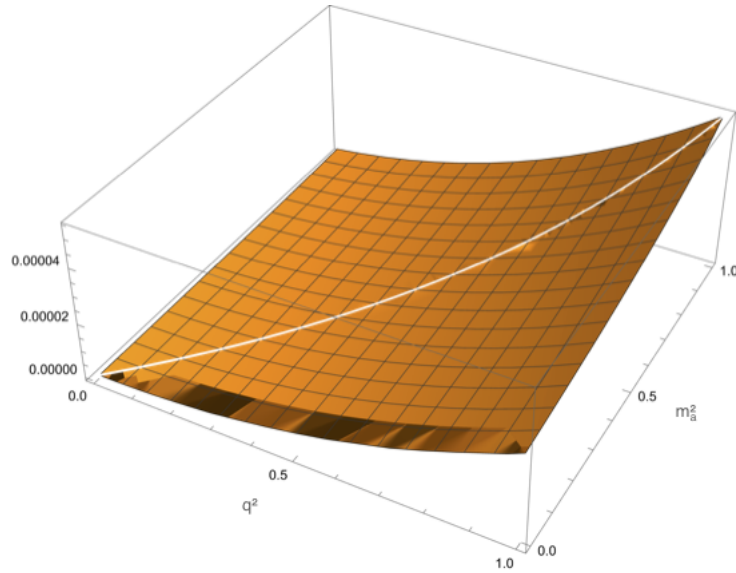

Figure 5.5: $|G_{loop}(q^2, m^2_a)|^2$ for one photon off-shell ($\pi^0 \rightarrow \gamma\gamma^*$)
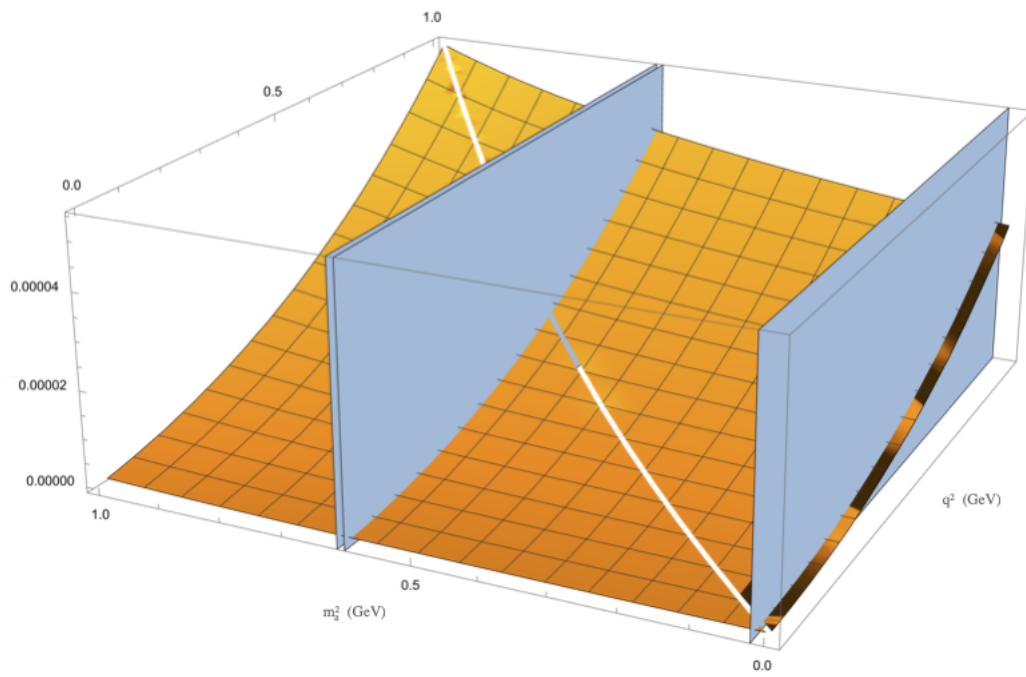
Figure 5.6: Regions of interest when $m_a^2 = m_\pi^2$ (blue vertical plane at the right), m_ρ^2, m_ω^2 (two blue vertical planes at the left)

Finally, an expression for the most general case where the two photons are off shell ($\pi^0 \to \gamma^*\gamma^*$) has been calculated as well, however, this expression is a function of three variables $G_{loop}(q^2, m_a^2, m_b^2)$ with no three dimensional visual representation, particular cases are the previous plots. A direct application of all these expressions will be given in Chapter 6.

5.3 Correction to coupling constant $g_{\rho\omega\pi}(q^2)$

Lowest-order pion decay amplitude $\mathcal{M}(\pi^0 \to \gamma\gamma)$ (Equation 5.1) can be manipulated as follows:
Considering $\Gamma_V(k_{1,2}^2 = 0) = 0$ for both vectorial particles, as well as final-state on-shell photons condition $k_1^2 = k_2^2 = 0$, as well as the transversality condition (Equation 2.16) $k_1^\nu \epsilon_\nu^*(k_1) = k_2^\chi \epsilon_2^*(k_2) = 0$, then the propagators transform into:

$$D_V^{\mu\nu}(k) = i \left(\frac{-g^{\mu\nu}}{-m_{\rho,\omega}^2} \right) \tag{5.20}$$

Reinserting into Equation 5.1 gives

$$\mathcal{M}^{(0)} = i g_{\rho\omega\pi} \left(\frac{4\pi\alpha}{g_\rho \, g_\omega} \right) k_1^\theta k_2^\tau \varepsilon^{\theta\tau\nu\chi} \epsilon_\nu^*(k_1) \, \epsilon_\chi^*(k_2) \tag{5.21}$$

Both amplitudes $\mathcal{M}^0$ and $\mathcal{M}^1$ (Equations 5.21 and 5.17 respectively, not explicit structure, see comments on G above) describe the exact same decay process $\pi^0 \to \gamma\gamma$, but $\mathcal{M}^0$ does it at first-order in $g_{\rho\omega\pi}$, while $\mathcal{M}^1$ does it at third order in $g_{\rho\omega\pi}$.
Both expressions can be combined to give

$$\mathcal{M} = \mathcal{M}^0 + \mathcal{M}^1 = \frac{g_{\rho\omega\pi} 4\pi\alpha}{g_\rho \, g_\omega} (1 + g_{\rho\omega\pi}^2 G_{loop}) k_1^\theta k_2^\tau \varepsilon^{\theta\tau\nu\chi} \epsilon_\nu^*(k_1) \, \epsilon_\chi^*(k_2) \tag{5.22}$$

Comparing with Equation 5.21 gives a correction for the coupling constant $g_{\rho\omega\pi}$, introducing the following notation:

$$g_{\rho\omega\pi}(q^2) \equiv \hat{g}_{\rho\omega\pi}(1 + \hat{g}_{\rho\omega\pi}^2 G_{loop}) \tag{5.23}$$

where $\hat{g}_{\rho\omega\pi}$ is the value at $q^2 = 0$, considering $q^2 = m_\pi^2 \approx 0$. This can be identified with the value obtained from $\pi^0 \to \gamma\gamma$ (Equation 5.13). The

corrected coupling constant $g_{\rho\omega\pi}(q^2)$ has an energy-dependence from G_{loop} from the incoming pion four-momentum $q = a + b$, as can be seen from Equation 5.15 and the different on-shell conditions for the photons.

As discussed in Chapter 2.3.2, these corrections come from an effective theory, that's the reason Equation 5.22 doesn't include higher-order corrections beyond $\mathcal{M}^{(1)}$. Therefore, the correction to the coupling for several scenarios has been obtained, which will be used in the next chapter to explore its implications.

Chapter 6

Application and results

As mentioned on the previous chapter, the general expression $g_{\rho\omega\pi}(q^2)$ is applied at the particular scattering process $e^+e^- \to \pi^0\pi^0\gamma$, where the two final state photons from the previous decay process $\pi^0 \to \gamma\gamma$ now play the role of the resonances ρ, ω, with different on-shell and off-shell conditions. The amplitude and the differential cross section are calculated, and the angular pion distribution is obtained. The chapter ends with the results showing Dalitz plots, angular distributions, differential cross sections and the energy dependent coupling constant $g_{\rho\omega\pi}(q^2)$.

6.1   Scattering process $e^+e^- \to \pi^0\pi^0\gamma$

A direct application of $g_{\rho\omega\pi}(q^2)$ and G_{loop} obtained in the previous chapter is found in the scattering process $e^+e^- \to \pi^0\pi^0\gamma$, illustrated in Figure 6.1. Just like the pion decay $\pi^0 \to \gamma\gamma$, this process has been already studied in the literature [30] and measured by experiments such as the SND collaboration [35, 36] and CDM2 [37]. This process involves two vertices similar to the one in $\pi^0 \to \gamma\gamma$. The first one considers both vector mesons (ρ, ω) off-shell and the second one just the omega off-shell. Here, the finite decay width effect of those resonances and the loop corrections obtained previously will be exhibit.

The uniqueness of this work resides in the consideration of an observable that may be sensitive to such effects, namely the angular distribution of one of the final state pions by performing a partial integration in the *phase space*, which is to be exposed in this current chapter.
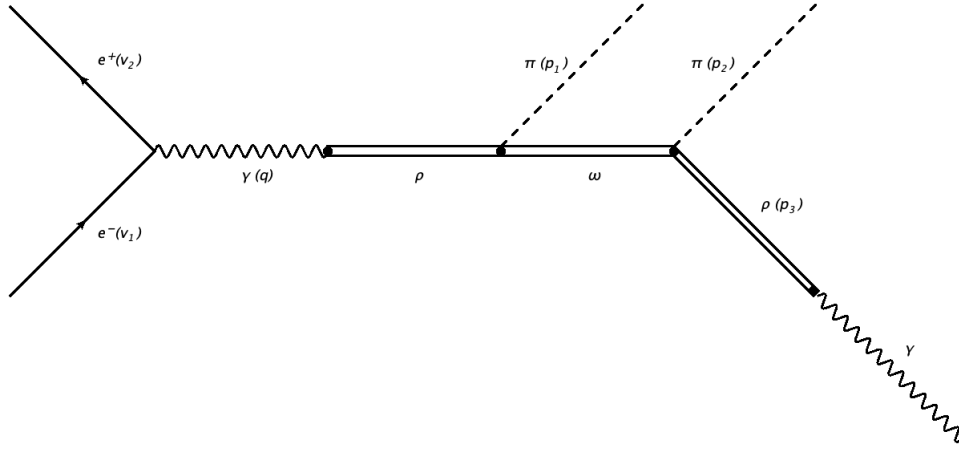
Figure 6.1: Scattering process $e^+e^- \to \pi^0\pi^0\gamma$ with intermediate meson states ρ^0, ω^0

The four-momenta notation used comes from Figure 6.1: $e^+(v_2)\, e^-(v_1) \to \pi^0(p_1)\, \pi^0(p_2)\, \gamma(p_3)$

Applying Feynman rules, the amplitude of this process is given by

$$\mathcal{M} = l^\mu M_\mu, \tag{6.1}$$

where l^μ is the *leptonic* part, which includes the factor coming from the photon propagator

$$l^\mu = -i\,e\,\bar{v}(v_2)\gamma^\tau u(v_1) \left(\frac{-i\,g^{\mu\tau}}{q^2} \right) \tag{6.2}$$

and M_μ is the hadronic part

$$
\begin{aligned}
M_\mu =&\, \epsilon_\rho^*(p_3) \left(-i\,e\frac{m_\rho^2}{g_\rho}g_{\rho\chi} \right) D_{\rho^0}^{\nu\chi}(p_3) i g_{\rho\omega\pi 1}\varepsilon^{\alpha\lambda\beta\nu}(q-p_1)^\alpha p_3^\beta \cdot \\
&\cdot D_{\omega^0}^{\lambda\gamma}(q-p_1)\,i\,g_{\rho\omega\pi 2}\varepsilon^{\sigma\delta\epsilon\gamma}q^\sigma(q-p_1)^\epsilon D_{\rho^0}^{\delta\theta}(q) \left(-i\frac{e\,m_\rho^2}{g_\rho}g_{\delta\mu} \right)
\end{aligned}
\tag{6.3}
$$

This time, the unstable propagators D_{ρ^0} and D_{ω^0} have their complete form, including the $im_V\Gamma_V$ term (Equation 5.2).

It's important to remark the distinction between the two different coupling constants $g_{\rho\omega\pi 1}$ and $g_{\rho\omega\pi 2}$. The former corresponds to the left vertex with pion $\pi(p_1)$ and the latter to the right vertex with pion $\pi(p_2)$.

Owing to the fact that resonant states are virtual particles, $g_{\rho\omega\pi 1}$ relates with the general case $G_{loop}(q^2, m_a^2, m_b^2)$ from Section 5.2.3, while $g_{\rho\omega\pi 2}$ corresponds to the particular case $G_{loop}(q^2, m_a^2)$, because $p_3^2 = 0$ by momentum conservation.

The squared amplitude has been calculated using *Feyncalc* [38, 39, 40], summing over lepton spin and photon polarization, in terms of scalar products of the four-momentum vectors. The result is a large expression in terms of the masses m_e, m_ρ, m_ω, decay widths $\Gamma_\rho, \Gamma_\omega$, coupling constant g_ρ (Equation 5.12), corrected coupling constants $g_{\rho\omega\pi 1}$, $g_{\rho\omega\pi 2}$ (Section 5.3) and the different scalar products between four-momentum of electron v_1, positron v_2, pions p_1, p_2, final-state on-shell photon p_3 and the internal four momentum $q = v_1 + v_2$.

$$|\mathcal{M}_{e^+e^-\to\pi^0\pi^0\gamma}|^2= -e^6 g_{\rho\omega\pi1}^2 g_{\rho\omega\pi2}^2 m_\rho^4(\Gamma_\omega^2 m_\omega^2 + (m_\omega^2 - 2(p_1 \cdot p_3) + q^2 - 2(q \cdot p_2))^2)$$
$$(m_e^2(m_\pi^2((p_2 \cdot p_3)^2 q^2 + 2(p_2 \cdot p_3)(q \cdot p_3)((q \cdot p_2) - 2q^2) + (q \cdot p_3)^2$$
$$(q^2 + 2(q \cdot p_2))) + m_\pi^4(-(q \cdot p_3)^2) - (p_2 \cdot p_3)^2(q^4 - 2q^2(q \cdot p_2)$$
$$+ 2(q \cdot p_2)^2) + 2(p_2 \cdot p_3)q^2(q \cdot p_2)(q \cdot p_3) - 2(q \cdot p_2)^2(q \cdot p_3)^2)$$
$$+ m_\pi^2(m_\pi^2(2q^2(v_1 \cdot p_3)(v_2 \cdot p_3) + (q \cdot p_3)^2(v_1 \cdot v_2)$$
$$- 2(q \cdot p_3)((q \cdot v_1)(v_2 \cdot p_3) + (q \cdot v_2)(v_1 \cdot p_3))) + (p_2 \cdot p_3)^2 q^2(v_1 \cdot v_2)$$
$$+ 2(p_2 \cdot p_3)(-(q^2((v_1 \cdot p_2)(v_2 \cdot p_3) + (v_1 \cdot p_3)(v_2 \cdot p_2))$$
$$+ (q \cdot p_3)(-(q \cdot p_2)(v_1 \cdot v_2) + (q \cdot v_1)((v_2 \cdot p_2) - 2(q \cdot v_2))$$
$$+ (q \cdot v_2)(v_1 \cdot p_2)) + (q \cdot p_2)((q \cdot v_1)(v_2 \cdot p_3) + (q \cdot v_2)(v_1 \cdot p_3)))$$
$$+ (q \cdot p_3)((q \cdot p_3)(q^2(v_1 \cdot v_2) - 2((q \cdot p_2)(v_1 \cdot v_2) + (v_1 \cdot p_2)(v_2 \cdot p_2))$$
$$+ 2(q \cdot v_1)(q \cdot v_2)) - 2q^2(q \cdot v_2)(v_1 \cdot p_3) + 2(q \cdot p_2)(v_1 \cdot p_3)(2(q \cdot v_2)$$
$$+ (v_2 \cdot p_2))) + 2(v_2 \cdot p_3)(q^4(v_1 \cdot p_3) - q^2(2(q \cdot p_2)(v_1 \cdot p_3)$$
$$+ (q \cdot p_3)(q \cdot v_1)) + (q \cdot p_2)((q \cdot p_3)(2(q \cdot v_1) + (v_1 \cdot p_2)) - (q \cdot p_2)(v_1 \cdot p_3))))$$
$$+ (p_2 \cdot p_3)^2(q^4(v_1 \cdot v_2) - 2q^2((q \cdot p_2)(v_1 \cdot v_2) + (q \cdot v_1)(q \cdot v_2)$$
$$- (v_1 \cdot p_2)(v_2 \cdot p_2)) + 2(q \cdot p_2)(2(q \cdot v_1)(q \cdot v_2) - (q \cdot v_1)(v_2 \cdot p_2)$$
$$- (q \cdot v_2)(v_1 \cdot p_2))) + 2(p_2 \cdot p_3)(-(q^4((v_1 \cdot p_2)(v_2 \cdot p_3) + (v_1 \cdot p_3)(v_2 \cdot p_2)))$$
$$+ q^2((q \cdot p_3)(-(q \cdot p_2)(v_1 \cdot v_2) + (q \cdot v_1)(v_2 \cdot p_2) + (q \cdot v_2)(v_1 \cdot p_2)$$
$$- 2(v_1 \cdot p_2)(v_2 \cdot p_2)) + (q \cdot p_2)((q \cdot v_1)(v_2 \cdot p_3) + (q \cdot v_2)(v_1 \cdot p_3)$$
$$+ 2(v_1 \cdot p_2)(v_2 \cdot p_3) + 2(v_1 \cdot p_3)(v_2 \cdot p_2))) - 2(q \cdot p_2)^2(-(q \cdot p_3)(v_1 \cdot v_2)$$
$$+ (q \cdot v_1)(v_2 \cdot p_3) + (q \cdot v_2)(v_1 \cdot p_3)))$$
$$- 2(q \cdot p_2)(q \cdot p_3)(-(v_1 \cdot p_3)(v_2 \cdot p_2)(q^2 - 2(q \cdot p_2))$$
$$+ (q \cdot p_3)(v_2 \cdot p_2)((q \cdot v_1) - 2(v_1 \cdot p_2)) + (q \cdot p_3)(q \cdot v_2)(v_1 \cdot p_2))$$
$$+ 2(q \cdot p_2)(v_2 \cdot p_3)(q^2 - 2(q \cdot p_2))((q \cdot p_3)(v_1 \cdot p_2)$$
$$- (q \cdot p_2)(v_1 \cdot p_3))) \, / \, q^4 g_\rho^4 m_\omega^2(\Gamma_\omega^2 + m_\omega^2)(\Gamma_\omega^2 m_\omega^2 + (-m_\omega^2 + m_\pi^2 + 2(p_1 \cdot p_3))^2)$$
$$(\Gamma_\rho^2 m_\rho^2 + (q^2 - m_\rho^2)^2)$$

$$\tag{6.4}$$

In practice, this equation has been exported as a *Fortran* input, and an algorithm capable of computing every the phase space integration on it has been written in the same programming language.

Similar to the previous calculation of the decay rate Γ_T (Equation 5.8) an expression of ρ decay width with energy-dependence $\Gamma_\rho(q)$ has been obtained

(using decay process $\rho^+ \rightarrow \pi^+ \pi^0$) and implemented to test how much the differential cross section varies between this and a constant decay width Γ_ρ.

$$\Gamma_\rho(q) = \frac{m_\rho^5 \, \Gamma_\rho \, (\lambda(q^2, m_\pi^2, m_\pi^2))^{1.5}}{q^{2.5} \, (\lambda(m_\rho^2, m_\pi^2, m_\pi^2))^{1.5}}, \tag{6.5}$$

where $\lambda(x, y, z) = x^2 + y^2 + z^2 - 2xy - 2xz - 2yz$ is the *Källen function*.

6.2 Pion angular distribution

Once the squared amplitude is obtained, Section 2.3.1 indicates the following step is to calculate the differential cross section, which is a purely kinematical procedure. Scattering process $e^+ e^- \rightarrow \pi^0 \pi^0 \gamma$ is a two-to-three bodies production process. Following Kumar's article [41], the kinematics for scattering process is given by the five Lorentz invariant kinematic variables

$$\begin{aligned}
s &\equiv s_0 = Q^2 \\
t_0 &= (v_1 - p_1)^2 \\
s_1 &= (Q - p_1)^2 \\
u_1 &= (Q - p_2)^2 \\
t_1 &= (v_1 - p_2)^2
\end{aligned} \tag{6.6}$$

where $Q \equiv v_1 + v_2$, $v_1^2 = v_2^2 \equiv m_e^2$. Using these definitions, the momentum conservation $v_1 + v_2 = p_1 + p_2 + p_3$ and the on-shell photon condition $p_3^2 = 0$, the scalar products are given by

$$Q \cdot v_1 = \frac{s}{2}$$

$$Q \cdot v_2 = \frac{s}{2}$$

$$Q \cdot p_1 = \frac{1}{2}(s + m_\pi^2 - s_1)$$

$$Q \cdot p_2 = \frac{1}{2}(s + m_\pi^2 - u_1)$$

$$Q \cdot p_3 = s - (Q \cdot p_1 + Q \cdot p_2)$$

$$v_1 \cdot v_2 = \frac{s}{2}$$

$$v_1 \cdot p_1 = \frac{1}{2}(m_\pi^2 - t_0)$$

$$v_1 \cdot p_2 = \frac{1}{2}(m_\pi^2 - t_1) \tag{6.7}$$

$$v_1 \cdot p_3 = v_1 \cdot v_2 - (v_1 \cdot p_1 + v_2 \cdot p_2)$$

$$v_2 \cdot p_1 = Q \cdot p_1 - v_1 \cdot p_1$$

$$v_2 \cdot p_2 = Q \cdot p_2 - v_1 \cdot p_2$$

$$v_2 \cdot p_3 = Q \cdot p_3 - v_1 \cdot p_3$$

$$p_1 \cdot p_3 = \frac{1}{2}(u_1 - m_\pi^2)$$

$$p_2 \cdot p_3 = \frac{1}{2}(s_1 - m_\pi^2)$$

$$p_1 \cdot p_2 = \frac{1}{2}(u_2 - 2m_\pi^2)$$

where the assumption $m_\pi^2 >> m_e^2 \approx 0$ has been established, and $u_2 = s - 2Q \cdot p_3$ is an auxiliary variable.

Following Kumar's notation, the phase-space is given by

$$\mathcal{P}_3 = \frac{1}{2}\pi \{\lambda(s, M_1^2, M_2^2)\}^{-\frac{1}{2}} \{s \cdot \lambda(s, M_1^2, M_2^2)\}^{-\frac{1}{2}} \cdot$$
$$\int_{s_{1-}}^{s_{1+}} ds_1 \left[\int_{u_{1-}}^{u_{1+}} du_1 \left[\lambda(s, s_1, m_\pi^2)\lambda(s, m_\pi^2, u_1) \right]^{-\frac{1}{2}} \right] \cdot$$
$$\cdot \int_{t_{0-}}^{t_{0+}} dt_0 \left[\int_{t_{1-}}^{t_{1+}} dt_1 \left[(1 - \xi_1^2)(1 - \eta_1^2)(1 - \zeta_1^2) \right]^{-\frac{1}{2}} \right] \cdot \tag{6.8}$$
$$\cdot F(s_1; u_1, t_1).$$

65

The limits of integration are

$$s_{1-} = m_\pi^2, \quad s_{1+} = (\sqrt{s} - m_\pi)^2$$

$$u_{1\pm} = s + m_\pi^2 - \frac{(s_1 + m_\pi^2)(s + s_1 - m_\pi^2)}{2s_1} \pm \frac{[\lambda(s, m_\pi^2, s_2)\lambda(s, s_1, m_\pi^2)]^{\frac{1}{2}}}{2s} \quad (6.9)$$

$$t_{1\pm} = m_e^2 + m_\pi^2 - \frac{s + m_\pi^2 - u_1}{2} \pm \frac{[\lambda(s, m_e^2, m_e^2)\lambda(s, m_\pi^2, u_1)]^{\frac{1}{2}}}{2s} X_{1\pm}$$

where

$$X_{1\pm} = \xi_1 \eta_1 \pm \left[(1 - \xi_1^2)(1 - \eta_1^2)\right]^{\frac{1}{2}}$$

$$\xi_1 = [s(s + m_\pi^2 - s_1) - 2s(m_e^2 + m_\pi^2 - t_0)][\lambda(s, m_e^2, m_e^2)\lambda(s, s_1, m_\pi^2)]^{-\frac{1}{2}}$$

$$\eta_1 = [2s(s_1 + m_\pi^2) - (s + m_\pi^2 - u_1)(s + s_1 - m_\pi^2)][\lambda(s, m_\pi^2, u_1)\lambda(s, s_1, m_\pi^2)]^{-\frac{1}{2}}$$

$$\zeta_1 = (\omega_1 - \xi_1\eta_1)[(1 - \xi_1^2)(1 - \eta_1^2)]^{-\frac{1}{2}}$$

$$\omega_1 = [s(s + m_\pi^2 - u_1) - 2s(m_e^2 + m_\pi^2 - t_1)][\lambda(s, m_e^2, m_e^2)\lambda(s, m_\pi^2, u_1)]^{-\frac{1}{2}}$$

$$(6.10)$$

The term $F(s_1; u_1, t_1)$ is the squared amplitude 6.4 from previous chapter. With all this information, the *angular pion distribution* between the initial-state particle $e^+(v_1)$ or $e^-(v_2)$ and the final state particle $\pi^0(p_1)$ (as seen from the center of mass frame) is given by

$$\frac{d\sigma}{d\zeta_0} \propto \frac{d\mathcal{P}_3}{d\zeta_0} = \frac{\pi}{4s} \int_{s_{1-}}^{s_{1+}} \frac{ds_1}{(1 - \xi_1^2)^{1/2}} \cdot$$

$$\cdot \int_{u_{1-}}^{u_{1+}} \frac{du_1}{[\lambda(s, m_\pi^2, u_1)]^{1/2}(1 - \eta_1^2)^{1/2}} \int_{t_{1-}}^{t_{1+}} \frac{dt_1}{(1 - \zeta_1^2)^{1/2}} \cdot \quad (6.11)$$

$$\cdot F(s, s_1; t_0(\zeta_0), t_1; u_1)$$

where $\zeta_0 = \cos\theta = \boldsymbol{p}_1 \cdot \boldsymbol{v}_1 / |\boldsymbol{p}_1||\boldsymbol{v}_1|$ is the angle between v_1 (or v_2) and p_1 as seen from the center of mass frame.

Comparing Kumar's phase space with the convention used in kinematic summary of Particle Data Group [8], a factor of $(2\pi)^9$ is missed ($n = 3$ for $e^+e^- \to \pi^0\pi^0\gamma$), thus, this factor is added here to set the equivalence.

$$d\Phi_n(P; p_1, ..., p_n) = \delta^4\left(P - \sum_{i=1}^n p_i\right) \prod_{i=1}^n \frac{d^3 p_i}{(2\pi)^3 2E_i} \quad (6.12)$$

$$d\sigma = \frac{(2\pi)^4 |\mathcal{M}|^2}{4\sqrt{(p_1 \cdot p_2)^2 - m_1^2 m_2^2}} \times d\Phi_n(p_1 + p_2; p_3, ..., p_{n+2}) \tag{6.13}$$

Substituting Equation 6.12 into Equation 6.13 ($m_1^2 = m_2^2 = m_e^2 \approx 0$) and comparing with Kumar's Phase Space 6.11 gives the final result

$$\frac{d\sigma}{d\zeta_0} = \frac{|\mathcal{M}|^2}{4(2\pi)^5 v_1 v_2} \cdot \frac{\pi |(s_{1+} - s_{1-})(u_{1+} - u_{1+})(t_{1+} - t_{1+})|}{4s\,\lambda(s, m_\pi^2, u_1)\sqrt{(1-\xi_1^2)(1-\eta_1^2)(1-\zeta_1^2)}} \tag{6.14}$$

This expression is the differential cross section with respect to the angle ζ_0, the squared amplitude $|\mathcal{M}|^2$ corresponds to Equation 6.4.

Just like the squared amplitude $|\mathcal{M}|^2$, the differential cross section $\frac{d\sigma}{d\zeta_0}$, as well as scalar products (6.7), the integration (6.9) and the auxiliary variables (6.10) have been computed using *Fortran*

In order to obtain the angular distribution, the scalar product $v_1 \cdot p_1$ from Equation 6.7 must be rewritten in terms of ζ_0 as

$$v_1 \cdot p_1 = E_{v_1} E_{p_1} - \zeta_0 |\bar{v}_1||\bar{p}_1| \tag{6.15}$$

The quantities E_{v_1}, E_{p_1}, $|\bar{v}_1|$, $|\bar{p}_1|$ are obtained at the center of mass frame

$$\begin{aligned}
E_{v_1} &= \frac{1}{2}\sqrt{s}, \\
E_{p_1} &= \frac{m_\pi^2 + s - s_1}{s\sqrt{s}}, \\
|\bar{v}_1| &= \frac{1}{2}\sqrt{s}, \\
|\bar{p}_1| &= \sqrt{E_{v_1}^2 - m_\pi^2}.
\end{aligned} \tag{6.16}$$

By doing this, the variable t_0 from Equation 6.10 acquires the form

$$t_0 = m_\pi^2 - 2(E_{v_1} E_{p_1} - \zeta_0 |\bar{v}_1||\bar{p}_1|) \tag{6.17}$$

Giving the freedom to choose a specific value for ζ_0 between $(-1, 1)$ for evaluation. In the following section, the results for several conditions are presented.
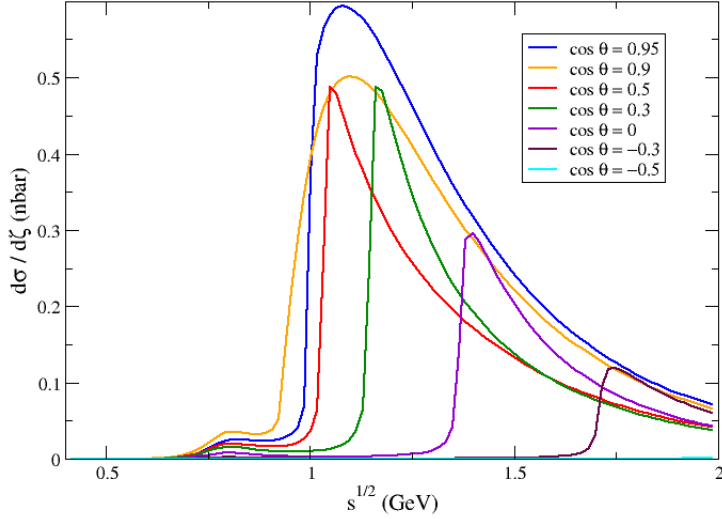
Figure 6.2: Differential cross sections for several values of $\zeta_0 = \cos\theta$ using a constant value $\Gamma_\rho = 0.1475$ GeV.

6.3 Results

Figure 6.2 shows the differential cross sections versus the energy from the center of mass $\sqrt{s}$ for several values of $\zeta_0 = \cos\theta$. These results have been computed using a constant value $g_{\rho\omega\pi1} = g_{\rho\omega\pi2} = 14.8162$ GeV^{-1} [30] and constant rho width $\Gamma_\rho = 0.1475$ GeV.

As can be seen, negative values are highly suppressed, like the light-blue line for $\zeta_0 = -0.5$. This is explained by picturing a final-state pion coming back from the same trajectory of the incident lepton (electron or positron) as seen from the center of mass frame, like a *recoil*, so it makes sense for values close to $\zeta_0 = -1$ to be highly suppressed, and emerge as they get closer to $\zeta_0 = 1$. Figure 6.3 shows the exact same differential cross sections from Figure 6.2, but this time using the energy dependent ρ width $\Gamma_\rho(q^2)$ from Equation 6.5. Figure 6.4 shows a comparison between both configurations at a particular value of $\cos\theta$, showing the effect of an energy dependent decay width.

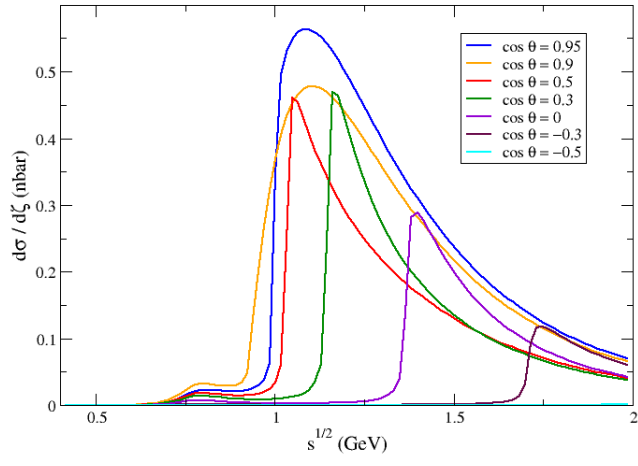The following aspect to notice is the presence of two *bumps*; the first one

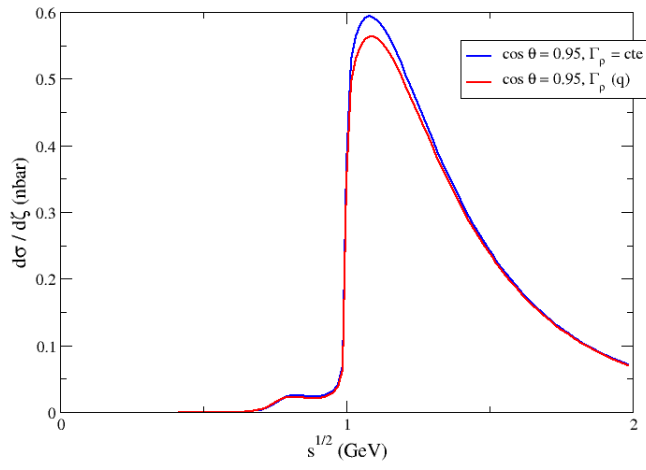Figure 6.3: Differential cross sections for numerous values of $\zeta_0 = \cos\theta$ using $\Gamma_\rho(q^2)$.

Figure 6.4: Comparison between differential cross sections using $\Gamma_\rho(q^2)$ and a constant value of Γ_ρ.
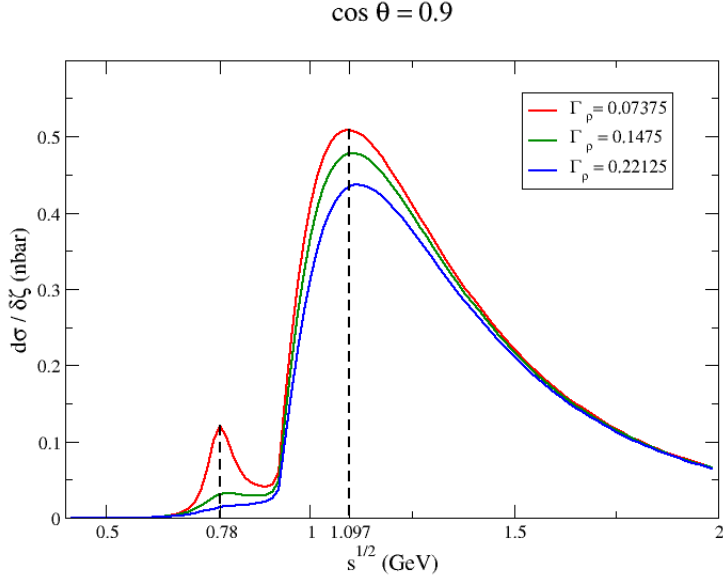
Figure 6.5: Differential cross sections for $\zeta_0 = 0.9$ using $\Gamma_\rho(q^2)$ with initial value of Γ_ρ as indicated (see Equation 6.5). Two bumps can be spotted.

is the little crest at $\sqrt{s} = 0.78$ GeV (Figure 6.5), and the second one is the biggest crest at $\sqrt{s} = 1.097$ GeV.

The former coincides with m_ρ, and that is precisely what is happening; when $s \equiv q^2 = m_\rho^2$, the first ρ particle is manifesting itself as a resonance, *i.e.* the entire cross section *resonates* due to the form of unstable propagators (Equation 5.2) of the ρ, but not the ω. The latter corresponds to the ω resonance which, since it is not explicitly dependent on s but s_1, is reflected at a higher energy.

Figure 6.6 is the *Dalitz* plot for s, s_1 variables (at $\cos\theta = 0.9$), where the amplitude weighted distribution of the differential cross section has been spotted, and it is evident how this time the cross section resonates at $\sqrt{s_1} = m_\omega = 0.78266$ GeV. There is a straight link between $s \leftrightarrow \rho$ and $s_1 \leftarrow \omega$.

Figure 6.7 shows the Dalitz region of $\sqrt{s}$, $\sqrt{s_1}$, *i.e.* all the values $\sqrt{s_1}$ can take given a particular value of s. Looking at $\sqrt{s} = m_\rho$, there are no values of $\sqrt{s_1} = m_\omega$, however, there are at $\sqrt{s} = 1.097$ GeV (maximum value from Figure 6.5). This explains the biggest crest from Figure 6.5; both ρ and ω
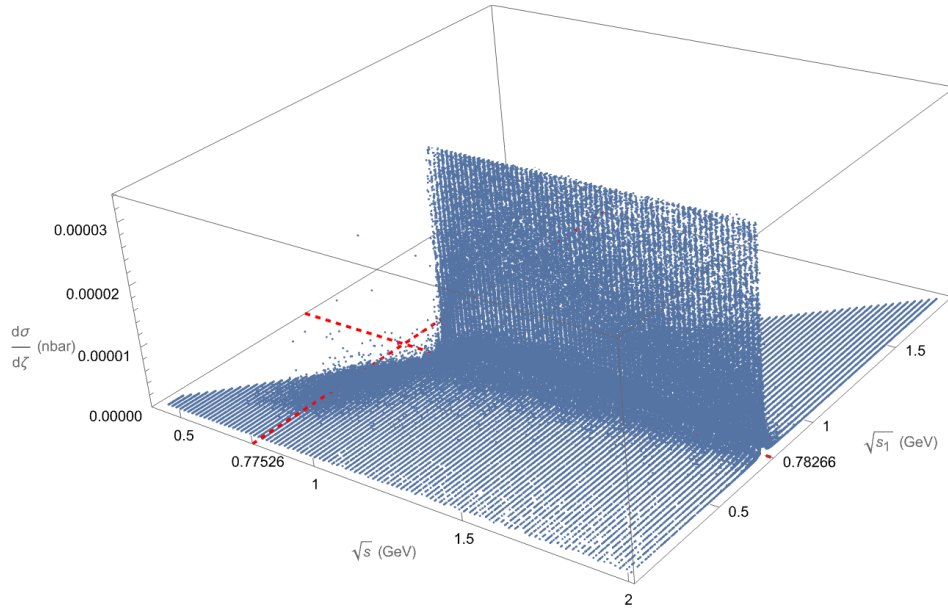
Figure 6.6: Dalitz plot for s and s_1 at $\cos\theta = 0.9$. It is evident how the cross section resonates at $m_\omega = 0.78266$ GeV

particles are resonating at the same time, although the ρ is off-shell, its large decay width allows it to make a sizeable contribution, manifesting it as a big amplitude. Another indicator of this is the fact that the biggest crest starts growing at the same energy $\sqrt{s_1} = m_\omega$ first "intersects" with $\sqrt{s} \approx 0.93$ GeV, corresponding with the opening of the $\omega - \pi$ channel on-shell.

Also, from Figure 6.7, by measuring the energy (in decay widths Γ_ρ) from m_ρ to $max = 1.097$ GeV, it gives $n = 2.15$. Plotting a vertical line the same energy to the right of the maximum value, and doing the same to $\sqrt{s_1} = m_\omega$ with horizontal lines, gives a rectangular region where both ρ_1 and ω resonate at the same time, considering their respective widths.

This analysis has been applied to $\cos\theta = 0.3$ as well (figure 6.8), obtaining similar conclusions. Figure 6.9 shows the distribution of $\sqrt{s}$ vs $\sqrt{s_1}$ for different angles, and as can be seen, for bigger angles, the allowed values of $\sqrt{s_1}$ increase as well.

Regarding $g_{\rho\omega\pi1}$ and $g_{\rho\omega\pi2}$ corrections (Equation 5.23), Figure 6.10 shows a comparison between $g_{\rho\omega\pi} = 11.2746$ GeV^{-1} and the energy-dependent versions of $g_{\rho\omega\pi1}, g_{\rho\omega\pi2}$ obtained for the corresponding conditions.

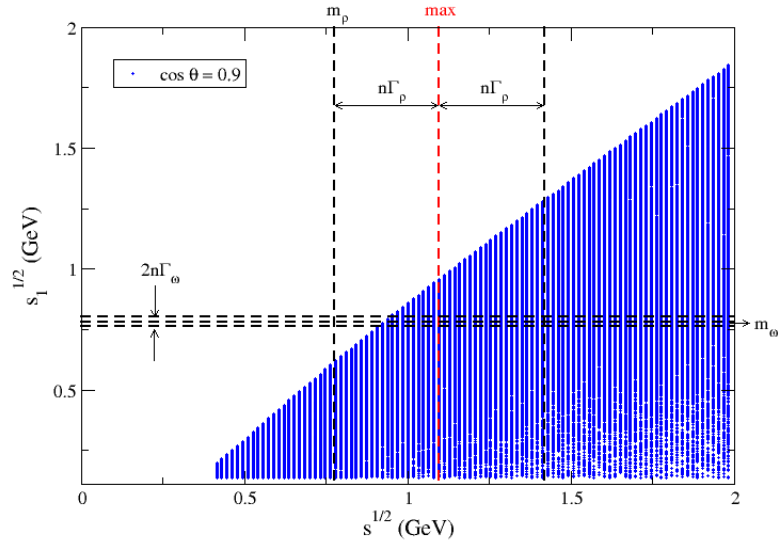Cross sections with a constant value of $g_{\rho\omega\pi1} = g_{\rho\omega\pi2} = 11.2746$ and corrected

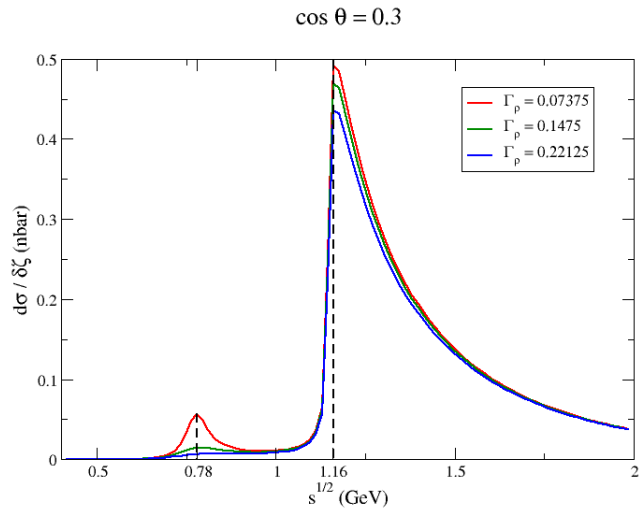Figure 6.7: Dalitz plot of variables $\sqrt{s_1}$, $\sqrt{s}$.

Figure 6.8: Differential cross sections for $\zeta_0 = 0.3$ using $\Gamma_\rho(q^2)$ with initial value of Γ_ρ as indicated
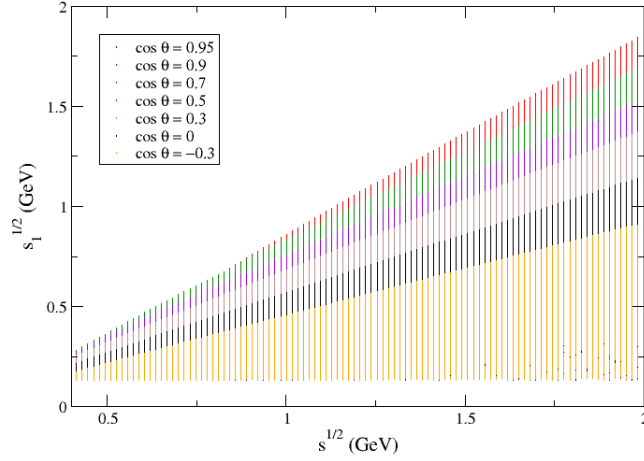
72

Figure 6.9: Dalitz region of $\sqrt{s}$, $\sqrt{s_1}$ for different angles. The allowed values of $\sqrt{s_1}$ increase as $\cos\theta$ increases.

versions of $g_{\rho\omega\pi1}$, $g_{\rho\omega\pi2}$ are shown in Figure 6.11. Plots are so similar is hard to distinguish between them, further discussion of this will be presented in the next section.

All plots from this section have been generated using software *Grace* and *Mathematica* [32].
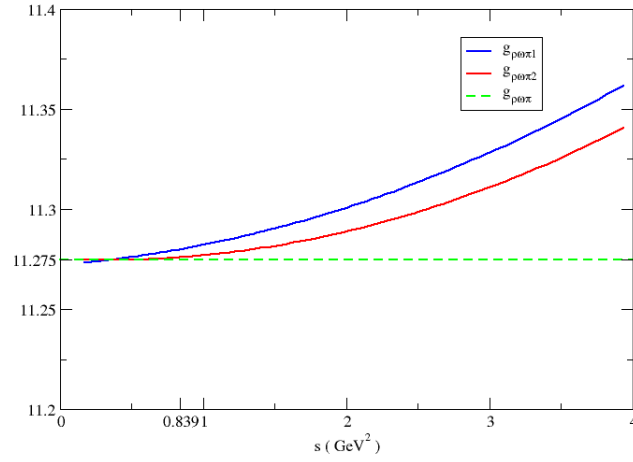
Figure 6.10: Comparison between coupling constant $g_{\rho\omega\pi}$ and corrected versions $g_{\rho\omega\pi1}, g_{\rho\omega\pi2}$
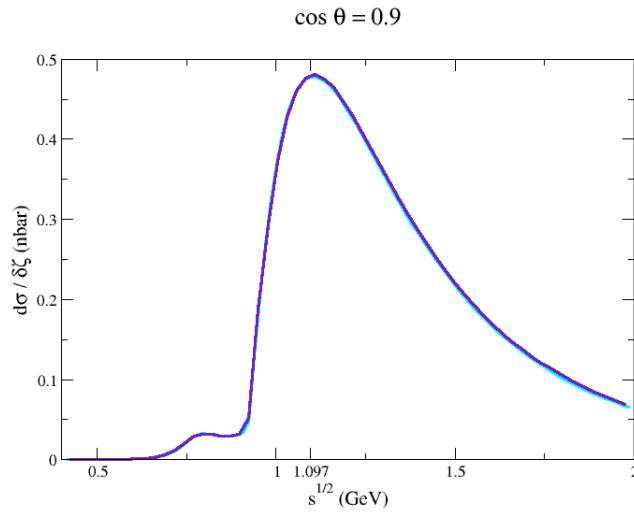

Figure 6.11: Differential cross sections for $\zeta_0 = 0.9$ using coupling constant $g_{\rho\omega\pi} = 11.2746$ (dark-blue plot) and using $g_{\rho\omega\pi1}, g_{\rho\omega\pi2}$ (light-blue plot) from equation 5.23

74

Chapter 7

Conclusions

Beginning with the decay process $\pi^0 \to \gamma\gamma$, where the two final photons are on-shell. By adding the third-order loop correction, or re-scattering correction (Figure 5.3) to the first order process (Figure 5.1), expressions $g_{\rho\omega\pi 1}, g_{\rho\omega\pi 2}$ have been obtained, and this has caused a modification to the constant value $g_{\rho\omega\pi} = 11.2746 \text{ GeV}^{-1}$, as Figure 6.10 suggest. For this can be concluded that, when final particles are on-shell, then the re-scattering process makes a significant contribution to the global coupling constant $g_{\rho\omega\pi}$. Of course, as mentioned in Section 2.3.2, these terms must be used with caution, as they diverge at larger energies, and their expressions have been obtained from an effective theory, meaning they should not be used for energies greater than a few GeV's.

Once the final photons are replaced with a general vectorial particle, then another two scenarios appear; final particles being both off-shell ($\gamma^*\gamma^*$) or a combination of on-shell off-shell ($\gamma\gamma^*$), which leads to the direct application exposed in Chapter 6, the scattering process $e^+e^- \to \pi^0\pi^0\gamma$

The second vertex $g_{\rho\omega\pi 2}$ is related to the later case, while the first vertex $g_{\rho\omega\pi 1}$ to the former one.

As can be seen from Figure 6.11, using a constant value $g_{\rho\omega\pi} = 11.2746$ GeV^{-1} and the corrected ones $g_{\rho\omega\pi 1}, g_{\rho\omega\pi 2}$ is generating practically the same cross section, it's hard to tell any difference between the two, by which can be concluded that these corrections are not of relevance for these particular scenarios.

Moving on with the cross section, it's evident from Figure 6.3 how bigger angles increase the amplitude, while angles close to $\cos\theta = -1$ are highly suppressed, as explained in Section 6.3, due to a recoil. What can be con-

cluded from these cross section plots is how the use of different constant values of Γ_ρ, as well as an energy-dependent $\Gamma_\rho(q^2)$ does affect the amplitude.

Finally, as explained in Section 6.3, ρ and ω are manifested as resonances, just like the W and Z bosons in the Higgs boson decay (Section 4.3). Mandelstam-like variables s and s_1 have spotted them in Figure 6.7, giving a proper explanation of the first and second crests from Figure 6.5; first one is the ρ resonating, while the second one are both ρ and ω resonating. Even though this phenomenon occurs at every angle, it's easier to find them at bigger angles, *i.e.* angles close to $\zeta_0 = \cos\theta = 1$

Summarizing, the effective coupling constant expression $g_{\rho\omega\pi}$ has been obtained from the pion decay process $\pi^0 \to \gamma\gamma$, and its final state photons have been generalized as ρ, ω resonances (by changing the initial conditions) in order to apply this expression to the particular scattering process $e^+e^- \to \pi^0\pi^0\gamma$. This expression has proven to be a significant correction when both final particles are on-shell, as discussed above.

The different initial parameters like the energy dependent decay widths $\Gamma_\rho, \Gamma_\omega$ and the scattered angle θ that appear on the unstable propagators (complex mass scheme) have been modified to test its dependence on the scattered amplitude, and see the effect they have on the angular distribution.

As the conclusions discussed above suggest, the specific objectives listed at the beginning of this work have been accomplished.

Chapter 8

Appendix

8.1 Appendix 1. Squared amplitude from pion decay $\pi \to \gamma\gamma$ with intermediate resonance states ρ, ω

Starting with Equation 5.3

$$
\begin{aligned}
i\mathcal{M}^{(0)} =& ig_{\rho\omega\pi}\varepsilon^{\theta\tau\mu\lambda}k_1^\theta k_2^\tau \left(i\frac{-g^{\mu\nu} + \frac{k_1^\mu k_1^\nu}{m_\rho^2 - i\, m_\rho\Gamma_\rho}}{k_1^2 - m_\rho^2 + i\, m_\rho\Gamma_\rho} \right) \cdot \\
& \cdot \left(i\frac{-g^{\chi\lambda} + \frac{k_2^\chi k_2^\lambda}{m_\omega^2 - i\, m_\omega\Gamma_\omega}}{k_2^2 - m_\omega^2 + i\, m_\omega\Gamma_\omega} \right) \left(-i\frac{e\, m_\rho^2}{g_\rho}g_{\nu\alpha} \right) \cdot \\
& \cdot \left(-i\frac{e\, m_\omega^2}{g_\omega}g_{\chi\beta} \right) \epsilon_\alpha^*(k_1)\epsilon_\beta^*(k_2)
\end{aligned}
\tag{8.1}
$$

Applying the on-shell photon condition $k_1^2 = k_2^2 = 0$, $\Gamma_V(k_{1,2}^2 = 0) = 0$, transversality condition $k_1^\nu \epsilon_\nu^*(k_1) = k_2^\chi \epsilon_\chi^*(k_2)$, contracting the remaining metric tensors, using $e^2 = 4\pi\alpha$ and simplifying what's left, then Equation 8.1 becomes

$$
i\mathcal{M}^{(0)} = ig_{\rho\omega\pi}\left(\frac{4\pi\alpha}{g_\rho g_\omega} \right) k_1^\theta k_2^\tau \varepsilon^{\theta\tau\nu\chi}\epsilon_\nu^*(k_1)\epsilon_\chi^*(k_2)
\tag{8.2}
$$

Squaring $|\mathcal{M}|^2$ implies multiplying by its complex conjugate and summing over polarizations. Using the property

$$\sum_{\text{pol}} \epsilon_\nu^* \epsilon_\delta = -g^{\nu\delta}, \tag{8.3}$$

then it gives

$$|\mathcal{M}|^2 = g_{\rho\omega\pi}^2 \left(\frac{4\pi\alpha}{g_\rho g_\omega}\right)^2 k_1^\theta k_2^\tau \varepsilon^{\theta\tau\nu\chi} k_1^\alpha k_2^\beta \varepsilon^{\alpha\beta\nu\chi}. \tag{8.4}$$

And finally, using

$$\varepsilon^{abcd} \varepsilon^{abkl} = 2(\delta_{ck}\delta_{dl} - \delta_{cl}\delta_{dk}) \tag{8.5}$$

gives an expression in terms of $k_1 \cdot k_2 = \frac{m_\pi^2}{2}$ which, after simplifying, gives Equation 5.4

$$|\mathcal{M}^{(0)}|^2 = g_{\rho\omega\pi}^2 \left(\frac{16\pi^2\alpha^2 m_\pi^4}{g_\rho^2 g_\omega^2}\right) \tag{8.6}$$

8.2   Appendix 2. Decay rate Γ from two-body decay

Following Kinematic review from Particle Data Group [8], two-body decay is given by

$$d\Gamma = \frac{1}{32\pi^2} |\mathcal{M}|^2 \frac{|\bar{p}_1|}{M^2} d\Omega \tag{8.7}$$

where, for the particular case where the pion decays into two on-shell photons $(m_1^2 = m_2^2, M = m_\pi)$

$$\begin{aligned} |\bar{p}_1|^2 &= \frac{1}{2M} \sqrt{\lambda(M^2), m_1^2, m_2^2} \\ &= \frac{1}{2M} \sqrt{M^4 + m_1^4 + m_2^4 - 2M^2 m_1^2 - 2M^2 m_2^2 - 2m_1^2 m_2^2} \\ &= \frac{1}{2m_\pi} \sqrt{m_\pi^4} \\ &= \frac{m_\pi}{2}. \end{aligned} \tag{8.8}$$

Substituting Equation 8.8 into Equation 8.7 and integrating over the entire solid angle ($d\Omega = 4\pi$), gives Equation 5.6

$$\Gamma = \frac{1}{16\pi} \frac{|\mathcal{M}|^2}{m_\pi} \tag{8.9}$$

Bibliography

[1] G. Aad et al. Observation of a new particle in the search for the standard model higgs boson with the ATLAS detector at the LHC. *Physics Letters B*, 716(1):1–29, sep 2012.

[2] Khépani Raya, Lei Chang, Adnan Bashir, J. Javier Cobos-Martinez, L. Xiomara Gutiérrez-Guerrero, Craig D. Roberts, and Peter C. Tandy. Structure of the neutral pion and its electromagnetic transition form factor. *Phys. Rev. D*, 93:074017, Apr 2016.

[3] H. L. L. Roberts, C. D. Roberts, A. Bashir, L. X. Gutiérrez-Guerrero, and P. C. Tandy. Abelian anomaly and neutral pion production. *Phys. Rev. C*, 82:065202, Dec 2010.

[4] Khépani Raya, Adnan Bashir, and Pablo Roig. Contribution of neutral pseudoscalar mesons to a_μ^{hlbl} within a schwinger-dyson equations approach to qcd. *Phys. Rev. D*, 101:074021, Apr 2020.

[5] M Gell-Mann. The eightfold way: A theory of strong interaction symmetry.

[6] David McMahon. *Quantum field theory demystified: A self-teaching guide.* 2009.

[7] Y. Ne'eman. Derivation of strong interactions from a gauge invariance. *Nuclear Physics*, 26(2):222–229, August 1961.

[8] R. L. Workman and Others. Review of Particle Physics. *PTEP*, 2022:083C01, 2022.

[9] Alan D. Martin Francis Halzen. *Quarks and Leptons: An Introductory Course in Modern Particle Physics.* Wiley, 1991.

[10] Barry R. Holstein John F. Donoghue, Eugene Golowich. *Dynamics of the Standard Model*. Cambridge University Press, 1992.

[11] David J. Griffiths. *Introduction to Elementary Particles*. Wiley-VCH, 2008.

[12] "J. J. Sakurai". Theory of Strong Interactions. *Annals of physics*, 11:1–48, 1960.

[13] Dieter Schildknecht. Vector meson dominance. 2005.

[14] Norman M. Kroll, T. D. Lee, and Bruno Zumino. Neutral vector mesons and the hadronic electromagnetic current. *Phys. Rev.*, 157:1376–1399, May 1967.

[15] Emmy Noether. Invariant variation problems. *Transport Theory and Statistical Physics*, 1(3):186–207, jan 1971.

[16] Reinhold A. Bertlmann. *Anomalies in Quantum Field Theory*. Oxford University Press, 1996.

[17] Ta-Pei Cheng, Ling-Fong Li, and David Gross. *Gauge Theory of Elementary Particle Physics*. Oxford University Press, 1985.

[18] Yoichiro Nambu. Quasi-particles and gauge invariance in the theory of superconductivity. *Phys. Rev.*, 117:648–663, Feb 1960.

[19] Jeffrey Goldstone. Field theories with ≪ superconductor ≫ solutions. *Il Nuovo Cimento (1955-1965)*, 19:154–164, 1961.

[20] J. Wess and B. Zumino. Consequences of anomalous Ward identities. *Phys. Lett. B*, 37:95–97, 1971.

[21] Edward Witten. Global aspects of current algebra. *Nuclear Physics B*, 223(2):422–432, 1983.

[22] "Vladimir Kuksa". Complex-Mass Definition and the Structure of Unstable Particle's Propagator. *Advances in High Energy Physics*, 2015:1–8, 2015.

[23] L A Jiménez Pérez and G Toledo Sánchez. Absorptive corrections for vector mesons: matching to complex mass scheme and longitudinal corrections. *Journal of Physics G: Nuclear and Particle Physics*, 44(12):125003, nov 2017.

[24] G. López Castro and G. Toledo Sánchez. Gauge invariance and finite width effects in radiative two-pion tau lepton decay. *Physical Review D*, 61(3), Jan 2000.

[25] G. López Castro, J. L. M. Lucio, and J. Pestieau. W± propagator on the resonance region. *Modern Physics Letters A*, 06(40):3679–3682, 1991.

[26] Nikolas Kauer and Giampiero Passarino. Inadequacy of zero-width approximation for a light higgs boson signal. *Journal of High Energy Physics*, 2012(8), aug 2012.

[27] Paul Langacker. *The Standard Model and Beyond*. Taylor Francis, 2017.

[28] M. E. Peskin. The electroweak standard model. 4. the standard model higgs boson, June 2016.

[29] The CMS Collaboration. Measurement of the Higgs boson width and evidence of its off-shell contributions to ZZ production. *Nat. Phys.*, 18:1329–1334, 2022.

[30] Gustavo Alejandro Avalos Valentín. Constantes de acoplamiento hadrónicas desde un análisis global. Master's thesis, 2019.

[31] Gustavo Ávalos Antonio Rojas, Marxil Sánchez, and Genaro Toledo. Role of the $\rho(1450)$ in low-energy observables from an analysis in the meson dominance approach. *Physical Review D*, 107:1–13, 2023.

[32] Wolfram Research, Inc. Mathematica, Version 13.2. Champaign, IL, 2022.

[33] Hiren H. Patel. Package-x.

[34] T. Hahn and M. Pérez-Victoria. Automated one-loop calculations in four and d dimensions. *Computer Physics Communications*, 118(2):153–165, 1999.

[35] M. N. Achasov et al. Recent results from snd detector at vepp-2m, 2000.

[36] M.N. Achasov et al. Study of the process $e^+e^- \to \eta\gamma$ in the center-of-mass energy range 1.07-2.00 gev. *Physical Review D*, 90(3), aug 2014.

[37] R.R. Akhmetshin et al. Update: A reanalysis of hadronic cross section measurements at CMD-2. *Physics Letters B*, 578(3-4):285–289, jan 2004.

[38] Vladyslav Shtabovenko, Rolf Mertig, and Frederik Orellana. FeynCalc 9.3: New features and improvements. *Computer Physics Communications*, 256:107478, nov 2020.

[39] Vladyslav Shtabovenko, Rolf Mertig, and Frederik Orellana. New developments in FeynCalc 9.0. *Computer Physics Communications*, 207:432–444, oct 2016.

[40] R. Mertig, M. Böhm, and A. Denner. Feyn calc - computer-algebraic calculation of feynman amplitudes. *Computer Physics Communications*, 64(3):345–359, 1991.

[41] Rajendra Kumar. Covariant phase-space calculations of n-body decay and production processes. *Phys. Rev.*, 185:1865–1875, Sep 1969.

[42] Peter Lichard. Vector meson dominance and the π^0 transition form factor. *Physical Review D*, 83(3), feb 2011.

[43] Ernestos N. Argyres, Wim Beenakker, Geert Jan van Oldenborgh, Ansgar Denner, Stefan Dittmaier, Jiri Hoogland, Ronald Kleiss, Costas G. Papadopoulos, and Giampiero Passarino. Stable calculations for unstable particles: restoring gauge invariance. *Physics Letters B*, 358(3-4):339–346, sep 1995.